# Dynamics of Nanoconfined Acetonitrile

By

Cassandra Norton

Submitted to the graduate degree program in Chemistry and the Graduate Faculty of the University of Kansas in partial fulfillment of the requirements for the degree of Master of Science.

_____

Chairperson Ward H. Thompson

_____

Brian B. Laird

_____

Timothy A. Jackson

Date Defended: 12-20-2010

The Thesis Committee for Cassandra Norton
certifies that this is the approved version of the following thesis:

Dynamics of Nanoconfined Acetonitrile

_____

Chairperson Ward H. Thompson

Date approved: 4-27-2011

## Abstract

The results of dynamics simulations of confined acetonitrile are presented. Confinement is achieved by filling previously formed silica pores having hydroxyl-terminated head groups with liquid acetonitrile. These pores are of the same nominal radius—1.2 nm—and have approximately the same surface coverage of hydroxyl groups, forming a hydrophilic surface. The three-site acetonitrile molecule with parameters previously tested was used for classical molecular dynamics simulations.

The main components of interest in the simulations are the diffusion coefficients and reorientational correlation times, two dynamical constants of a given system, and the causes of the magnitudes and variability of each is explored. The acetonitrile molecules are first tested in the bulk system and are shown to yield reasonable results and then are confined in order to extract more information regarding dynamical changes when confinement occurs.

Drastic changes are seen when the solvent is confined. The mean squared displacement is used to find the diffusion coefficient both for the whole system and for molecules separated according to where they sit relative to the pore wall or the *z*-axis. Both of these analyses were performed for calculating the reorientation time by using the reorientational autocorrelation function and then fitting those curves to multi-exponential and stretched exponential functions.

## Acknowledgements

The writer wishes to thank her fellow group members, A. A. Vartia and C. M. Morales in particular, for the lively discussions that led to valuable insights and her extremely patient advisor, W. H. Thompson.

Funding for this research was provided by the National Science Foundation (Grants CHE-0518290 and CHE-1012661).

# Table of Contents

**Abstract** ..... iii

**Acknowledgements** ..... iv

**Table of Contents** ..... v

**Chapter 1: Introduction** ..... 1
- **1. Optical Kerr effect spectroscopy** ..... 2
- **2. Quasi-elastic neutron scattering** ..... 2
- **3. Nuclear magnetic resonance** ..... 2

**Chapter 2: Methods** ..... 5
- **1. System** ..... 5
- **2. Molecular Dynamics Simulations** ..... 9
- **3. Diffusion Coefficient and Reorientational Correlation Constants** ..... 10

**Chapter 3: Diffusion Coefficient** ..... 13
- **1. Results** ..... 13
  - 1.1. Bulk versus Confined ..... 13
    - 1.1.1. Mean-squared displacement ..... 15
    - 1.1.2. Velocity Autocorrelation ..... 17
  - 1.2. Pore Heterogeneity ..... 18
    - 1.2.1. Directional Differences ..... 18
    - 1.2.2. Across the Pores ..... 19
    - 1.2.3. Layers ..... 21
  - 1.3. Pore Charge Effects ..... 30
  - 1.4. Temperature Effects ..... 33
- **2. Discussion** ..... 38
  - 2.1. Bulk versus Confined ..... 38
  - 2.2. Across the Pores ..... 40
  - 2.3. Layers ..... 40
  - 2.4. Pore Charge Effects ..... 44
  - 2.5. Temperature Effects ..... 45

**Chapter 4: Reorientational Correlation Times** ..... 47
- **1. Results** ..... 47
  - 1.1. Bulk versus Confined ..... 47
  - 1.2. Pore Heterogeneity ..... 50
    - 1.2.1. Across the Pores ..... 50
    - 1.2.2. Layers ..... 51
  - 1.3. Pore Charge Effects ..... 61
- **2. Discussion** ..... 65
  - 2.1. Bulk versus Confined ..... 65
  - 2.2. Pore Heterogeneity ..... 66
    - 2.2.1. Across the Pores ..... 66
    - 2.2.2. Layers ..... 67
    - 2.2.3. Pore Charge Effects ..... 70

**Chapter 5: Conclusions** ..... 72
- **1. Diffusion coefficient** ..... 72

**2. Reorientational Correlation ..... 74**
**3. Future Work ..... 76**

**Bibliography ..... 77**

# Chapter 1: Introduction

Dynamic properties of bulk liquid systems have been well characterized, however considerably less is known at the molecular level of their nanoconfined counterparts. Confinement in materials such as zeolites, supramolecular assemblies, sol-gels, vesicles, proteins and reverse micelles can lead to dramatic differences in dynamical properties when contrasted with bulk liquids. The differences can be due to the fact that the surface to volume ratio is much higher in confined liquids so surface interactions become a large contributor to overall dynamics and geometric constraints obstruct the dynamics. The focus of this research is the dynamical properties of sol-gel confined acetonitrile.

Confinement may be relevant in various applications including catalysis, sensing, lubrication, oil recovery, cellular dynamics, microfluidic technology and molecular separation.[1] Because synthesis techniques are increasing in sophistication, confining structures can be tailored to be more efficient and therefore greener and less expensive. However, little is known about the molecular dynamics of nanoconfined liquids.

Experimental approaches such as optical Kerr effect spectroscopy, quasi-elastic neutron scattering measurements, NMR, second harmonic & sum frequency spectroscopy, Raman spectra and radioactive tracers have all been employed to probe the dynamics of confined liquids.[2-8]

## 1. Optical Kerr effect spectroscopy

By using optical Kerr effect spectroscopy, reorientation times for a liquid can be calculated by experiment. The method is highly sensitive and selective.[10] In it, polarization spectroscopy geometry is implemented. A pump pulse polarized at 45° that is used in excitation then a probe pulse with a variable time delay is vertically polarized. The analyzer is set to detect horizontally polarized light, so if the refractive index of the sample is isotropic, no signal is detected. However, if birefringence is induced by the pump pulse that leads to depolarization, a signal is recorded. The negative time derivative of the orientational correlation function for all of the molecules is proportional to the optical Kerr effect response.[2]

## 2. Quasi-elastic neutron scattering

Quasi-elastic neutron scattering (QENS) is a technique that directly probes single-molecule diffusion motion.[5] The data collected is analyzed in terms of Lorentizan components that include rotational and diffusive parts.[11] The level of response using this technique is related to the amount of movement by the atom or molecule of interest.[5] Distinguishing molecules according to placement within a confined framework is not possible using this method.[5]

## 3. Nuclear magnetic resonance

Nuclear magnetic resonance (NMR) spin-lattice relaxation has been used to find relaxation times of simple molecular liquids.[12] Direct information about the molecular dynamics is unavailable, however. NMR line shape is used to analyze the molecular

structure and can be used to probe the possibility of a bimodal nature of confined liquid molecules.[12]

Though these methods are useful and have their merits, a more complete knowledge of molecular movement can be obtained by utilizing molecular dynamics simulations. The experimental methods can then be used for comparison purposes – both for the theorist and the experimentalist. In experiments, direct causes of changes in dynamics when a liquid is confined are difficult to elucidate. Also, the ability to extract information on specific molecules within the confined network is not yet available.

Theoretical simulations and calculations can explain the origins of signals obtained in an experiment. Experimental data has led to a model to represent the behavior of confined molecules. Analysis of signals showed that dynamics of confined liquids changed dramatically from the bulk behavior for at least a fraction of the confined molecules. When experimentalists considered their data, the results often, though not always, coincided with a two-state model prediction.[3, 13] When curve fitting, analysis may include setting a time scale value to one known; that is, in this case, if a long time scale and a short time scale is seen, one may set the short time scale to the known bulk liquid time scale value. A two-state model has two assumptions. The first is that the molecules can be divided into two sets – those interacting with the confining framework, or wall, and those in the interior of the pore. The second characteristic for this model is those molecules that are in the interior of the pore exhibit bulk-like behavior.

Because the molecules of a confined liquid do show heterogeneity, a two-state model is a reasonable starting point for studying the system due to its simplicity.

However, the two-state model does not account for all of the information gathered, so a deeper probe into the cause of anomalous data is necessary to explain the true dynamics of the system. Computer experiments are especially useful in confined environments or when investigating solid-liquid interfaces. Direct experimental probes of molecular-level dynamics are still lacking and computational simulations are useful because they can fill in these gaps. For instance, even though molecular reorientation of a confined solvent can be probed experimentally, assigning the root causes of the changes in reorientation times remains a difficult task. Deciding if a molecule's reorientation time is due to surface electrostatic interaction or if it is related solely to steric hindrance is simple in a computer simulation but practically impossible for an experimentalist.

The research described in this thesis focuses on the combination of information contained in experimental data and computer simulations of nanoconfined acetonitrile. This includes, for example, answering the question of the core cause of reorientational correlation times. The two-state model description is tested, and dynamical properties are assigned based on confined solvent layers, starting at two—merely surface molecules versus interior molecules. In order to understand properties of a confining system, the movement of molecules in the framework must be known so the behavior of the solvent and the causes of the behavior are studied.[8] The deeper understanding of how a liquid moves when confined may lead to the design of new or more efficient porous materials.

# Chapter 2: Methods

In this work, the structure and dynamics of liquid acetonitrile have been examined using molecular dynamics (MD) simulations. Both bulk and nanoconfined liquid acetonitrile systems were constructed and simulations were run to obtain diffusion coefficients and reorientational correlation constants. Correlation functions were utilized to find the values of the parameters.

## 1. System

Classical molecular dynamics (MD) simulations of both bulk and nanoconfined liquid acetonitrile were carried out using the DL POLY package.[14] Bulk simulations involved 500 acetonitrile molecules at a density of 0.764 g/cm$^3$ (box length equaled 35.4672022326 Å). This value was based on the model proposed by Gee and van Gunsteren[15] and the simulations were carried out with cubic periodic boundary conditions.

Ten previously developed[16,17] amorphous silica pore models provided the framework for confinement of the liquid acetonitrile. These pores had a rigid silica ($SiO_2$) framework with surface silanol groups, SiOH and $Si(OH)_2$, that have fixed bond lengths but variable angles. The number of acetonitrile molecules in each pore was determined by the grand canonical Monte Carlo simulations of Gulmen and Thompson.[16,17] Briefly, the density was obtained by setting the confined $CH_3CN$ in equilibrium with the bulk liquid in Monte Carlo simulations where $CH_3CN$ molecules were added if it was energetically favorable to do so, sometimes leading to molecules trapped in the pore structure. The total number of confined $CH_3CN$ molecules varied

from 136 to 155 across the ten pores (see **Table 2.1**). The linear three-site ANL model (**Figure 2.1**) with the parameters[16] used in **Table 2.2** was used to describe the acetonitrile interactions. The total dipole of acetonitrile was 4.37 D.[15] The bond lengths and bond angles for this model were rigid. The Lennard-Jones and Coulombic interactions defined the potential energy $V(r_{ij})$ (**Eq 2.1**) between two site on different molecules:

$$V(r_{ij}) = 4\varepsilon_{ij}\left[\left(\frac{\sigma_{ij}}{r_{ij}}\right)^{12} - \left(\frac{\sigma_{ij}}{r_{ij}}\right)^{6}\right] + \frac{q_i q_j}{r_{ij}} \qquad (2.1)$$

where $\varepsilon$ is the Lennard-Jones potential well depth, $\sigma$ is the distance at which the Lennard-Jones interatomic potential is zero, $r_{ij}$ is the distance between the two atoms $i$ and $j$ and $q_i$ is the charge on the $i^{th}$ atom.

| | number of acetonitrile molecules | number of silanol moieties[16] |
|---|---|---|
| Pore 01 | 153 | 56 |
| Pore 02 | 136 | 60 |
| Pore 03 | 148 | 48 |
| Pore 04 | 145 | 58 |
| Pore 05 | 148 | 72 |
| Pore 06 | 153 | 72 |
| Pore 07 | 155 | 56 |
| Pore 08 | 146 | 86 |
| Pore 09 | 152 | 42 |
| Pore 10 | 149 | 40 |

**Table 2.1** The molecule/moiety count is presented among the pores of the same nominal radius of ~12 Å . The numbering of the pores is random.

The ten roughly cylindrical pores used in these simulations are all of the same nominal radius (~12 Å) with a length of 30 Å and cubic periodic boundary conditions in three dimensions. The Lennard-Jones parameters for the pore atoms are listed in **Table**

**2.2**. The oxygen $\sigma$ is theoretically large enough to encompass the hydrogen $\sigma$, but a small, weak interaction potential had to be considered for it to prevent instability during the simulation.[17] A sample pore is shown in **Figure 2.2**. A Lewis structure representation of the –(OH)-terminated and –$(OH)_2$-terminated silica is shown in **Figure 2.3**.

| Atom | $\varepsilon$ ( $^{kJ}/_{mol}$) | $\sigma$ (nm) | q (e) |
|---|---|---|---|
| Me | 1.336 | 0.348 | 0.287 |
| C | 0.35 | 0.3287 | 0.1376 |
| N | 0.35 | 0.319 | -0.4246 |
| Si | 0.00043367 | 0.250 | 1.280 |
| O (frame) | 0.01981751 | 0.270 | -0.640 |
| O (silanol) | 0.00737191 | 0.307 | -0.740 |
| H (silanol) | 0.00001586 | 0.1295 | 0.420 |

**Table 2.2** Parameters for acetonitrile molecule and pore frame atoms:[15] $\varepsilon$ - potential well depth, $\sigma$ - distance at which inter-atom potential is zero and $q$ – the atomic charge.

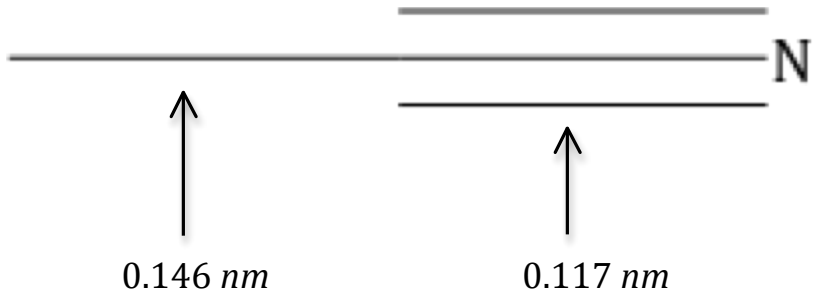


**Figure 2.1** The Lewis structure using the line-angle representation of acetonitrile is shown; the C-C-N angle is 180°.

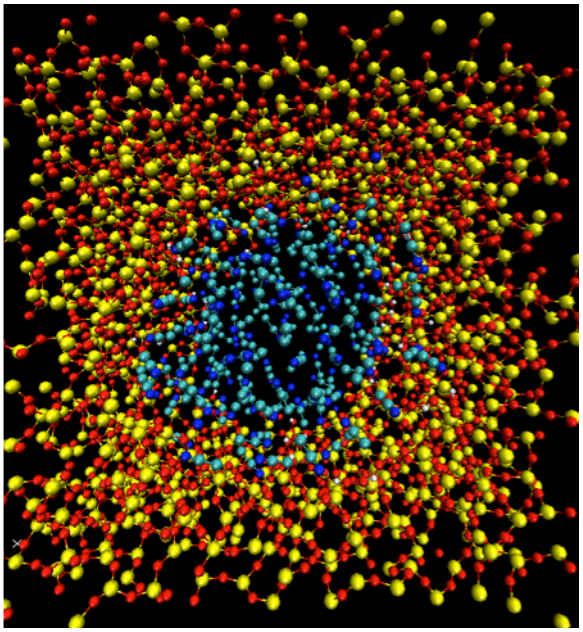

**Figure 2.2** A snapshot of pore 01 is displayed with the pore wall shown in red (oxygen), yellow (silicon) and white (hydrogen) and filled with acetonitrile solvent (the dark blue spheres are nitrogen and the light blue represent the carbon and the methyl groups in $CH_3CN$). The positive *z*-axis is pointing toward the viewer.

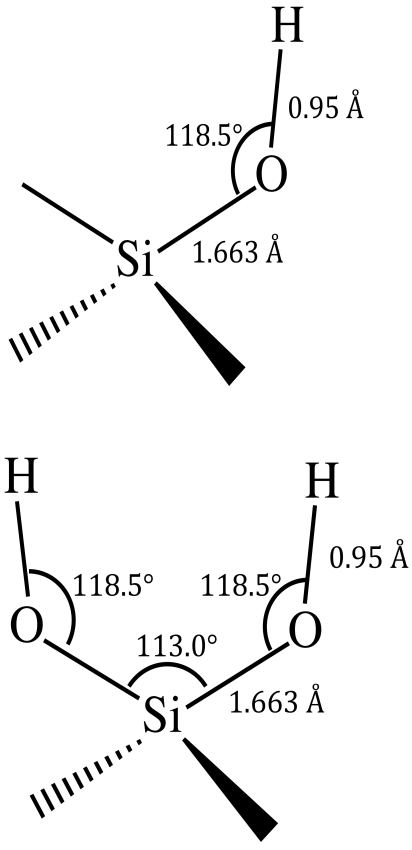


**Figure 2.3** The pore structure groups of silanol (top) and geminal silanol (bottom) are shown. Silicon is bonded to network oxygen atoms where the bonds are available.

Both hydrophilic and hydrophobic pores were studied. The hydrophilic pores are terminated with hydroxyl groups present as silanol, SiOH, or geminal, $Si(OH)_2$, with a surface coverage of 3 – 6 ($OH/nm^2$).[16,17] Hydrophobic pores were studied by removing the charges of the pore. It then becomes a completely neutral pore surface. This allows studying the effects of surface chemistry without changing the effective radius or the number of $CH_3CN$ molecules. Though the pores were similar, they are distinct from one another in size and surface coverage of silanol groups in order to have simulations that were as realistic as possible. The functionality is in close agreement with experimental functionality estimates, and the effect of this variation was compared among the pores.

## 2. Molecular Dynamics Simulations

The length of the MD trajectories used varied from 2 ns for the bulk liquid to 20 ns for confined acetonitrile. All were preceded by at least a 1 ns equilibration stage. A Nose-Hoover thermostat was used with a relaxation constant of 1.0 ps to maintain temperature in the NVT ensemble. Simulations were carried out at three temperatures, 275 K, 300 K and 325 K, though all analyses except temperature comparisons were at 300 K. All trajectories used a 2 fs time step, and the coordinates were saved every 80 fs for bulk $CH_3CN$ and every 40 fs for confined $CH_3CN$. The quaternion tolerance was set at $1.0 \times 10^{-4}$. The required cutoff for all forces was set to 10.0000 Å and the Verlet neighbor list shell width that specifies primary 'neighbors' to a given molecule was set to 2.0000 Å.

For the bulk simulations, a longer trajectory was not found to be necessary due to a lack of long time-scales. The total simulation time, including a 1 ns equilibration, was

3 ns. Long-range electrostatic interactions were included using an Ewald summation[15] with a convergence parameter of 0.243. Each *k*-vector had a maximum *k*-value index equal to 6.

In the confined systems, trajectories were run for 5 ns or longer. In order to calculate long time-scales for reorientation, 20 ns trajectories were used. The time step was also 2 fs, but the coordinates were saved only once every picosecond. Again, long-range electrostatic interactions were included by an Ewald summation, but the maximum *k*-value index in the *x* and *y* directions was 10 and in the *z* direction, along the pore axis, was 8.

## 3. Diffusion Coefficient and Reorientational Correlation Constants

In order to find the effect on acetonitrile dynamics upon confinement of the liquid, bulk simulations were carried out to calculate two values: the self-diffusion coefficient and the reorientational correlation time. Diffusion coefficients were calculated using the mean-squared displacement of the center-of-mass and velocity autocorrelation. The Einstein relation for center-of-mass RMS displacement is:[15]

$$D = \lim_{t \to \infty} \frac{\left\langle \left| \vec{r}(t) - \vec{r}(0) \right|^2 \right\rangle}{6t} \qquad (2.2)$$

where $D$ is the diffusion coefficient in three dimensions and $\vec{r}(t)$ is the vector-direction of acetonitrile at time $t$. The value of the diffusion coefficient was found by graphing the numerator of **Eq. (2.2)** versus time. The slope of that graph should then equal $6D$. For comparison, the velocity autocorrelation function is also utilized to find diffusion constants within a system using the equation:[9]

$$D = \frac{1}{3}\int_0^\infty dt\langle \vec{v}(t) \bullet \vec{v}(0)\rangle \quad (2.3)$$

for which $\vec{v}(t)$ is the center-of-mass velocity of an acetonitrile molecule at time *t*.

To compute the second quantity of interest, the reorientational correlation times ( $\tau_l$), the $l^{th}$ reorientational correlation function is calculated as:[15]

$$C_l(t) = \langle P_l(\vec{e}(t) \bullet \vec{e}(0))\rangle \quad (2.4)$$

where $P_l$ is the $l^{th}$-order Legendre polynomial and $\vec{e}(t)$ is the unit vector along the acetonitrile $H_3C - C \equiv N$ axis, arbitrarily pointing toward nitrogen.

Determining the diffusion constant or reorientational correlation time from the mean squared displacement or $C_l(t)$ for confined acetonitrile poses some difficulties, and many methods were explored to find the most reliable values. In the bulk liquid, however, a single-exponential decay function was fit to the reorientational correlation function:[15]

$$C_l(t) = A\exp\left(-\frac{t}{\tau_l}\right) \quad (2.5)$$

in order to calculate the reorientational correlation times of bulk acetonitrile. The time scale over which the reorientational autocorrelation was fit was determined by the length of time the function took to reach zero. Confined acetonitrile has more than one time scale so multi-exponential fits and stretched exponentials were tested to find the reorientational correlation times.

The results were further analyzed to explore how the time scales depend on the position of the molecule within the pore. Separating molecules according to where they are both relative to the pore wall and at different radii from the center of the pore to obtain dynamical information was also studied. For instance, if a $CH_3CN$ molecule was

within a certain distance of the pore wall, its diffusion coefficient would be calculated and averaged with the other acetonitrile molecules that were also within that distance of the pore wall. Then another group of molecules that were found in the next layer of the liquid in the pore would be similarly analyzed. See **Figure 3.7** in the following chapter for a diagram of this method. Because the molecules are not static in a simulation, they are likely to switch across layers. For any given analysis, the layer for a given molecule was chosen at the beginning of the correlation. If a molecule was in layer one at time step zero then it is considered to be part of layer one until the end of the correlation time. The maximum correlation time was 1 ns.

The final method by which dynamical information was obtained was to consider directional dynamics. Because the acetonitrile was confined in the *x*- and *y*-directions, but was "open" via periodic boundary conditions in the *z*-direction, the movement in the *z*-direction was studied relative to the other two dimensions to examine anisotropy in the diffusion coefficients.

For each of these calculations, error bars were obtained by block averaging. Each trajectory was separated as if it were multiple trajectories. For example, the 5 ns confined trajectory was split into eight 625-ps blocks that were each analyzed in the same way as the full-length trajectory. Then the standard deviation found among the calculated values of the blocks was used with the Student t-value to obtain error bars at the 95% confidence level. The equation[18] used to find the height of the error bars is $\Delta = t\sqrt{\sum_{i=1}^{n}(x_i - \bar{x})^2} \Big/ n(n-1)$ (**Eq. 2.6**) where $t$ is the Student $t$-value, $x$ is the value of the correlation function and $n$ is the number of blocks.

# Chapter 3: Diffusion Coefficient

The data obtained from the simulations of bulk and confined acetonitrile were analyzed to obtain insight into the influence of confinement on the dynamics. The mean squared displacement was calculated for every $CH_3CN$ simulation including the bulk liquid, the confined liquid in all of the hydrophilic pores, and the confined liquid in all ten hydrophobic pores. The results were also separated according to where the molecule was found with respect to the radial distance from the pore axis and the distance from the pore wall. All of these data were analyzed and the diffusion coefficient for each case was obtained.

To check the validity of the values obtained using the mean squared displacement, the velocity auto-correlation function was utilized and the diffusion coefficient was calculated from that function as well for the bulk and one hydrophilic pore simulation.

## 1. Results

### 1.1. Bulk versus Confined

A practical concern when moving from bulk to confined acetonitrile was to find the general trends of the dynamics constants upon confinement. Before analyses could be performed, some practical details had to be considered. For instance, the Monte Carlo simulations that were used to create the acetonitrile-filled pores added acetonitrile to any open volume, even if that volume was not truly accessible to the rest of the pore space. As a result, some of the molecules were caught in the silica framework in voids unconnected with the pore volume. These molecules cannot be used as part of the

confined data analysis as they would not reasonably model molecules in a real system where the pores are filled by immersion in a liquid or capillary condensation. In order to remove these molecules, a simulation was run in a pore with no charges on the pore framework. The maximum radial distance traveled of each acetonitrile molecule was calculated in the charge-neutral pore over 5 ns. The charges were removed so that electrostatics would not be a cause of immobility. The maximum radial movement of each molecule is shown graphically in **Figure 3.1** for pore 01.

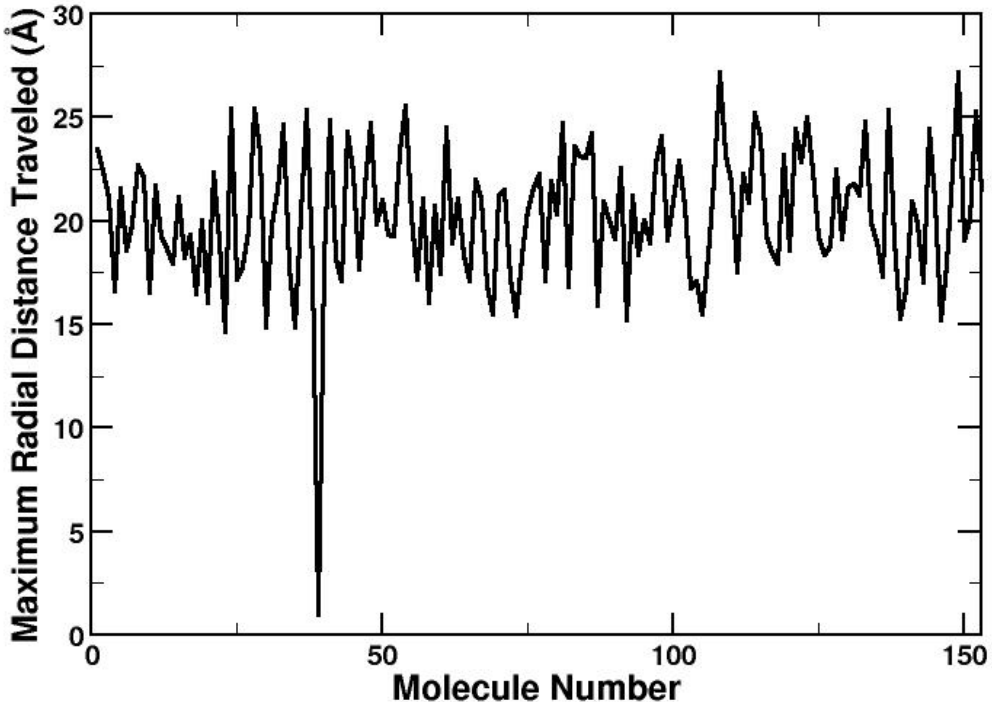


**Figure 3.1** illustrates the maximum radial distance traveled by each molecule in neutral Pore 01. The sharply dipped point is due to molecule number 39.

From **Figure 3.1**, one can easily see that a single molecule (in this case, molecule number 39) does not move in the same way as the others. An analogous graph was created for every pore, and after examination, a cutoff of 5 Å seems sufficient to distinguish immobilized versus free molecules. That is, if a molecule moves less than 5 Å radially in 5 ns then it is likely caught in the pore framework. For all of the

proceeding work, this criteria was used to remove the immobilized molecules from the sample pool.

### 1.1.1. Mean-squared displacement

The mean-squared displacement (MSD) can be seen in **Figure 3.2**. Both the bulk $CH_3CN$ and confined $CH_3CN$ (in pore 01) MSDs are shown. Obviously, the slope of the confined displacement is much smaller than that of the bulk. Another aspect of this graph is the similarity between the slopes at very short times (less than 0.5 ps) before the two curves diverge. At these values, the curves are quadratic. The bulk curve represents the average squared displacement over all of the acetonitrile molecules present, while the confined curve is the average over the acetonitrile molecules that are not immobilized in the silica pore wall framework. The error bars shown on the graph represent a 95% confidence range for the true average squared displacement for the bulk and for pore 01. The equations of the lines of best fit restricted to times between 2 and 10 ps can be seen in **Table 3.1**. Using this information and **Eq. 2.2**, the diffusion constant can be calculated, and the value is tabulated in the third column of **Table 3.1**.

The most obvious trend seen in **Table 3.1** is the difference between diffusion coefficients when comparing bulk to confined $CH_3CN$. When going from bulk to confined acetonitrile, the diffusion coefficient decreases significantly, by 73%. The confined *z*-direction diffusion coefficient is also much smaller than the bulk in the same direction – by 67%.

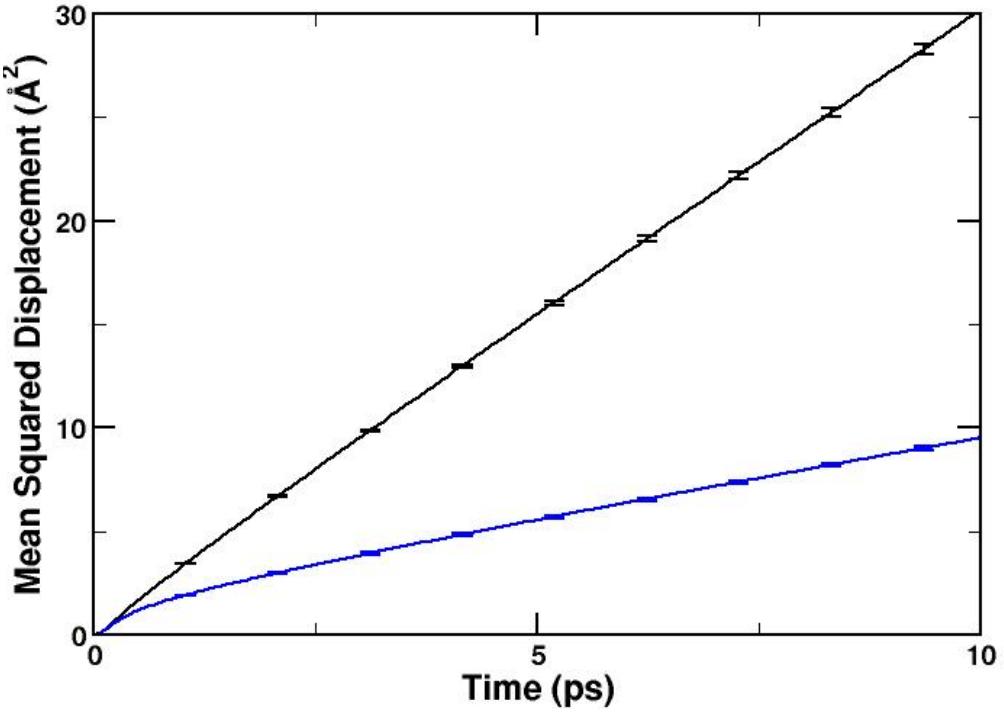


**Figure 3.2** The MSD function is plotted as a function of time for bulk (black) and confined (blue) acetonitrile with error bars representing a 95% confidence that the true mean is within their ranges.

| | Linear Fit | | Diffusion Coefficient $\left(\times 10^{-9}\, m^2/s\right)$ |
|---|---|---|---|
| | slope | intercept | |
| bulk | 2.95 | 0.656 | 4.91(8) |
| confined | 0.818 | 1.41 | 1.36(4) |
| bulk (*z* only) | 0.988 | 0.226 | 4.9(2) |
| confined (*z* only) | 0.327 | 0.502 | 1.64(5) |
| confined (*x* only) | 0.243 | 0.482 | 1.22(5) |
| | Velocity Autocorrelation Integral $\left(\times 10^{-9}\, m^2/s\right)$ | | |
| bulk | 15.4 | | 5.13(7) |
| confined | 4.77 | | 1.55(3) |

**Table 3.1** Linear fits of the mean-squared displacement graphs with respective diffusion coefficients. The numbers in parentheses represent the standard deviation in the final digit using 8 blocks.

### 1.1.2. Velocity Autocorrelation

Another way to find the diffusion coefficient is by using the velocity autocorrelation function. In this case, integrating the area under the curve will be used to find the value (**Eq. 2.3**) of the coefficient. The velocity autocorrelation graph is seen in **Figure 3.3**. The blue curve again represents the velocity autocorrelation of the confined acetonitrile while the black is representative of bulk acetonitrile. The confined curve was calculated using a 5 ns trajectory and the curve representing bulk acetonitrile was calculated using a 2 ns trajectory. The error bars for both curves were calculated

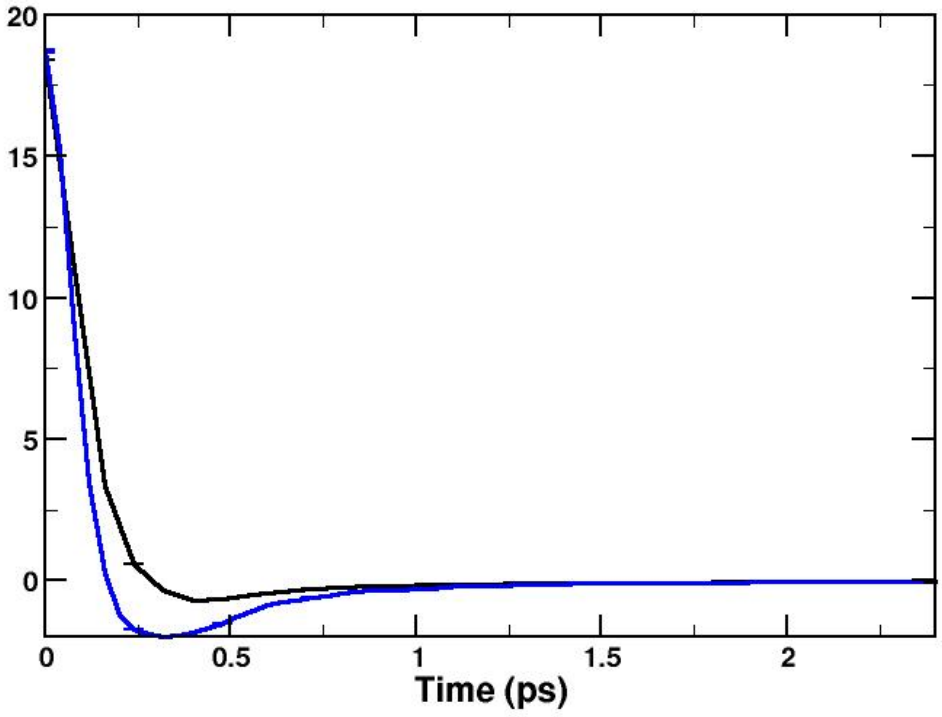


**Figure 3.3** The velocity autocorrelation is shown. The blue curve represents confined liquid acetonitrile and the black curve represents bulk liquid acetonitrile.

using block averaging over eight blocks. Both had block data sets that overlapped nearly perfectly so the error bars are nearly indistinguishable. The confined velocity

autocorrelation function decreases at a much faster pace than the bulk curve initially causing it to decrease well below zero before finally increasing back to zero at about 1.5 ps, approximately the same time as the bulk curve reaches zero again. This large negative component decreases the confined $CH_3CN$ diffusion constant. **Table 3.1** in the previous section summarizes the values of the diffusion constants calculated using the velocity autocorrelation function.

The diffusion coefficients that are found by using mean-squared displacement and by using the velocity autocorrelation function are not identical but are in good agreement. The relative difference between the bulk values going from the MSD to the velocity autocorrelation value is decreasing by 4%. Similarly, the relative difference between the confined values is 18%. Because the same trend is seen and similar values are calculated using either MSD or velocity autocorrelation, MSD will be utilized to calculate diffusion coefficients for the following trials.

## 1.2. Pore Heterogeneity

### 1.2.1. Directional Differences

A difference does exist between the diffusion in the *z*-direction as opposed to diffusion in the *x*- or *y*-directions. In the bulk system, all of the directions are the same. Within error, the MSD lines in the direction of *x*, *y* and *z* are the same. Similarly for the confined system, the *x*- and *y*-curves are the same. However, the diffusion coefficient in the *z*-direction is larger than the *x*-direction coefficient by 34% when confined. The graph showing this information is in **Figure 3.4**. Values for the diffusion coefficient were calculated using this figure and can be found in **Table 3.1**. Values for the *y*-direction were omitted due to their similarity to *x*.

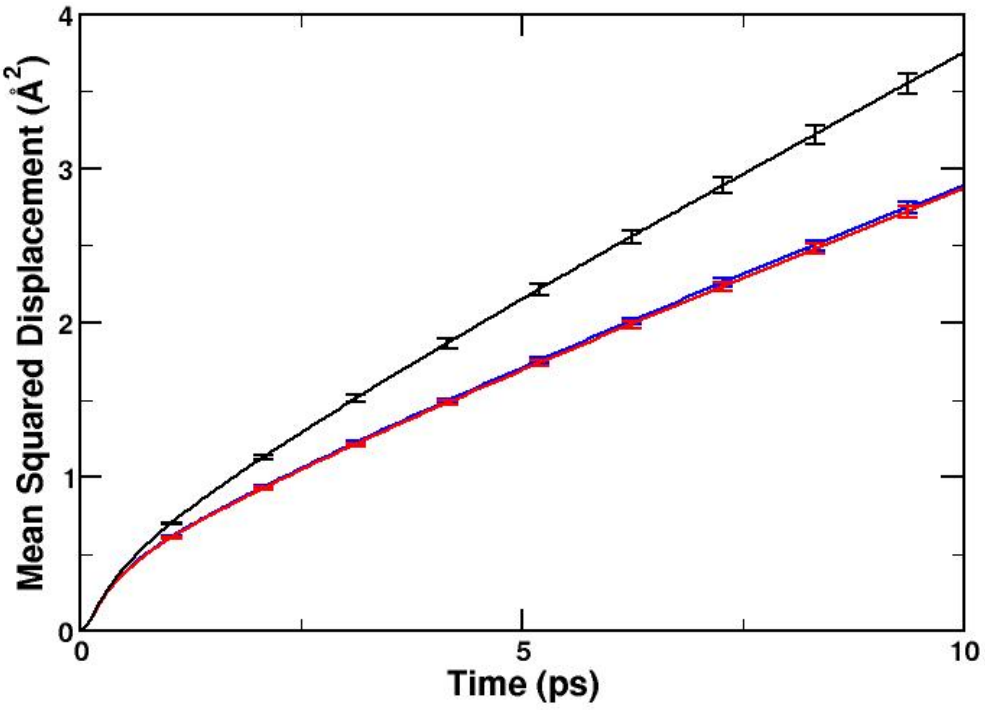


**Figure 3.4** shows the mean squared displacement by dimension in Pore 01. The red and blue lines represent diffusion in the *x*- and *y*-directions, respectively, and the black curve represents molecular diffusion in the *z*-direction.

### 1.2.2. Across the Pores

Each pore, though constructed in the same fashion, differs in the precise atomic-level structure and therefore has a slightly different diffusion constant. The MSD graph across the pores is shown in **Figure 3.5**. If any one of these curves were compared to the bulk system, the same trend seen in **Figure 3.1** would be evident. That is, the slope is much smaller for any confined displacement than that of the bulk acetonitrile. The main curves of importance in **Figure 3.5** are the black (approximately in the middle of the group), the dark blue (the top curve, or one with the largest slope which corresponds to pore 02) and the pink (the bottom curve, or the one with the smallest slope which corresponds to pore 08). The black line corresponds to pore 01 and was chosen as the example confined pore for the majority of analysis due in part to it yielding what

appears to be a representative sample of the pores. Values for the diffusion coefficient can be found in **Table 3.2** on the next page.

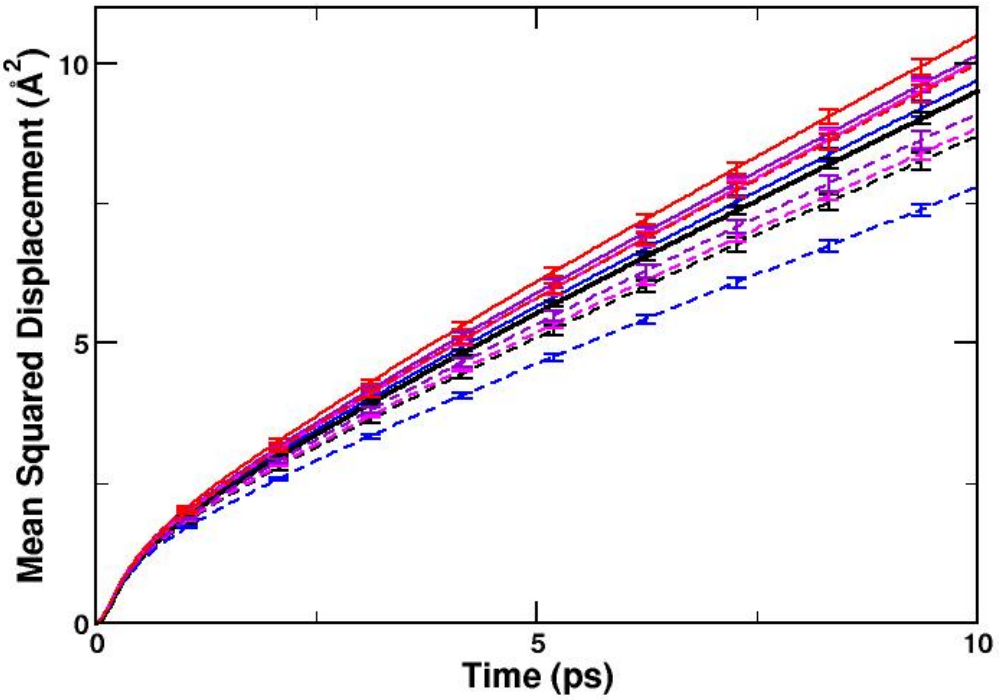


**Figure 3.5** The MSD functions are shown for 10 pores of ~12 Å radius. They are colored as follows: 01 (solid black), 02 (solid red), 03 (solid blue), 04 (solid violet), 05 (solid pink), 06 (dashed black), 07 (dashed pink), 08 (dashed blue), 09 (dashed violet) and 10 (dashed red).

The relative difference between the largest diffusion coefficient (in pore 08) and the smallest (in pore 02) is 28%.

| | linear fit | | Diffusion Coefficient $\left(\times 10^{-9}\, m^2/s\right)$ |
|---|---|---|---|
| | slope | intercept | |
| Pore 01 | 0.818 | 1.41 | 1.36(4) |
| Pore 02 | 0.908 | 1.50 | 1.51(3) |
| Pore 03 | 0.834 | 1.43 | 1.39(3) |
| Pore 04 | 0.877 | 1.45 | 1.46(3) |
| Pore 05 | 0.870 | 1.40 | 1.45(4) |
| Pore 06 | 0.742 | 1.34 | 1.24(3) |
| Pore 07 | 0.755 | 1.36 | $1.26(2_5)$ |
| Pore 08 | 0.651 | 1.33 | $1.09_5(2_5)$ |
| Pore 09 | 0.777 | 1.40 | 1.29(3) |
| Pore 10 | 0.861 | 1.44 | 1.43(3) |
| Average | 0.809 | 1.41 | 1.35 |
| Std. Dev. | 0.078 | 0.05 | 0.13 |

**Table 3.2** Diffusion coefficients from linear fits between 2-10 ps for the ten ~12 Å pores are tabulated. The numbers in parentheses indicate the error (one standard deviation in the final digit using 8 blocks).

### 1.2.3. Layers

Slight differences are seen between pores, but even larger differences are apparent when diffusion coefficients are calculated from different areas within a single pore. The criterion for determining the location of the molecule was categorized in two ways; these can be seen pictorially in **Figures 3.6** and **3.7**. In **Figure 3.6**, the property that determines in which layer a molecule belongs is where that molecule is relative to

the central *z*-axis, the axis along which the pore is oriented, at the beginning of its block (using block averaging). This is fairly simple. If the pore is separated into 1 Å layers in this way, then a molecule that is within 1 Å of the central axis at time zero is considered to be in the first layer. Similarly, if it is between 1 and 2 Å of the central axis at time zero, it is in the second layer. This continues until no more solvent molecules are in the layer, meaning the pore framework has been reached. The dotted lines in **Figure 3.6** that are spaced evenly relative to the central z-axis (denoted by the solid middle line) schematically represent the layers.

The second way to separate the molecules into layers is by considering them relative to the wall of the pore structure. Because the oxygen atoms are fairly evenly dispersed along the wall and are the atoms that also protrude into the solvent (as diols and silanols), the layers are made based on the nearest oxygen atom.[16,17] This is shown in **Figure 3.7**. Again if the layers have a width of 1 Å, then those acetonitrile molecules that are between 1 and 2 Å of an oxygen atom define the first layer. For the analysis, the nitrogen atom on the acetonitrile molecule is what governs the placement of the molecule. Due to potential interactions, no molecules are present within one angstrom of any oxygen molecules. The next layer is that which is between 2 and 3 Å from the

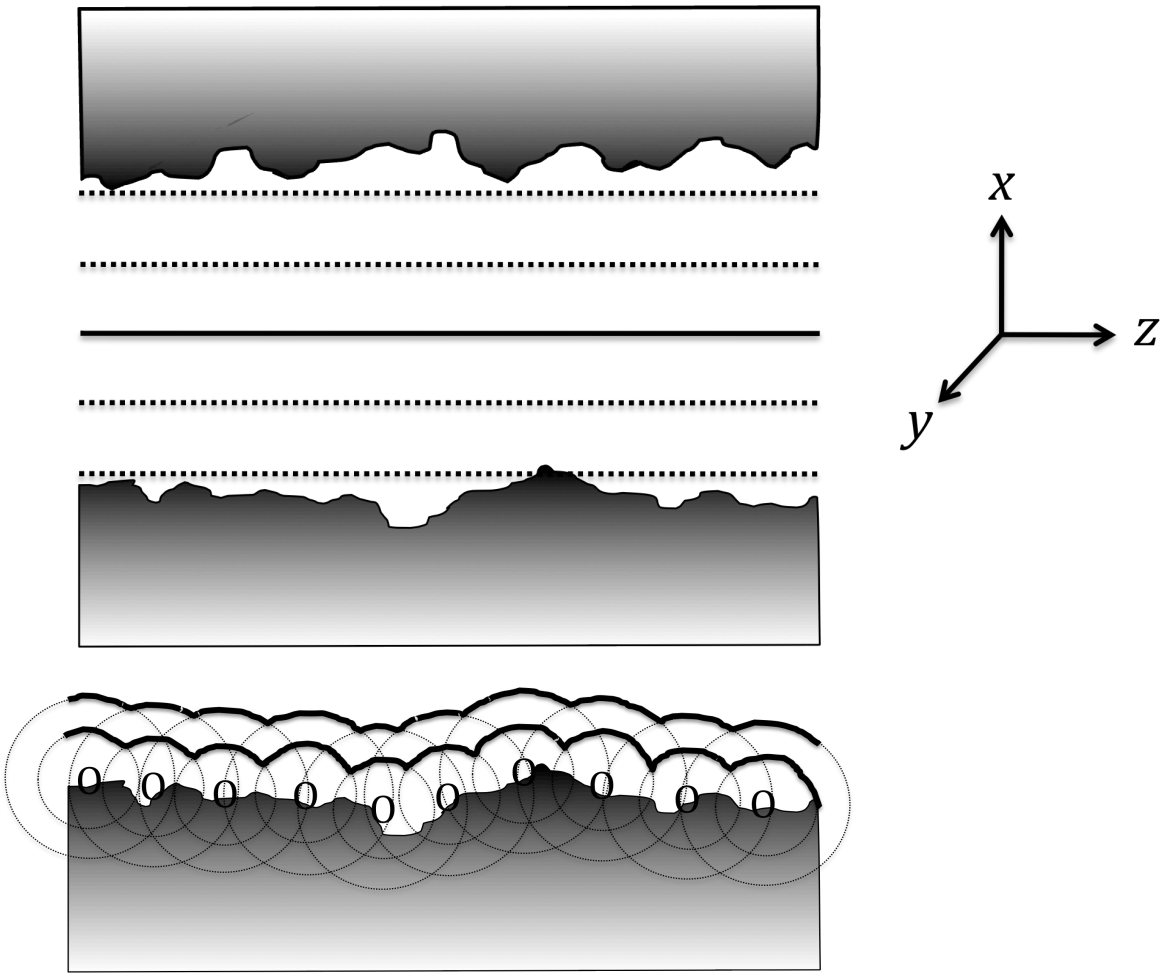


**Figures 3.6** and **3.7** show a schematic representation of the two methods of layering – radially and by distance to nearest pore structure oxygen, respectively.

nearest oxygen and so forth until the molecules that are the farthest away from any oxygen are accounted for. Presumably those molecules will be located somewhere in the center, but that is not necessary using this method of separation.

Both of these methods of layering were considered when analyzing the data. The first, which is much simpler, was performed for the initial analysis. The graph of the results can be seen in **Figure 3.8**. The solid blue curve with the large slope represents the molecules that are in the first layer that had three or greater molecules included on average to calculate the curve's slope, or those theoretically closest to the center of the pore. The trend of the slopes is that they decrease as they move away from the center of

the pore. A table of the slopes with respective diffusion coefficients can be seen in **Table 3.3**. In the final column of this table, a percent contribution of each curve is given. These values are all given for pore 01, in which the farthest molecules from the center were at a distance of between 13 and 14 Å.

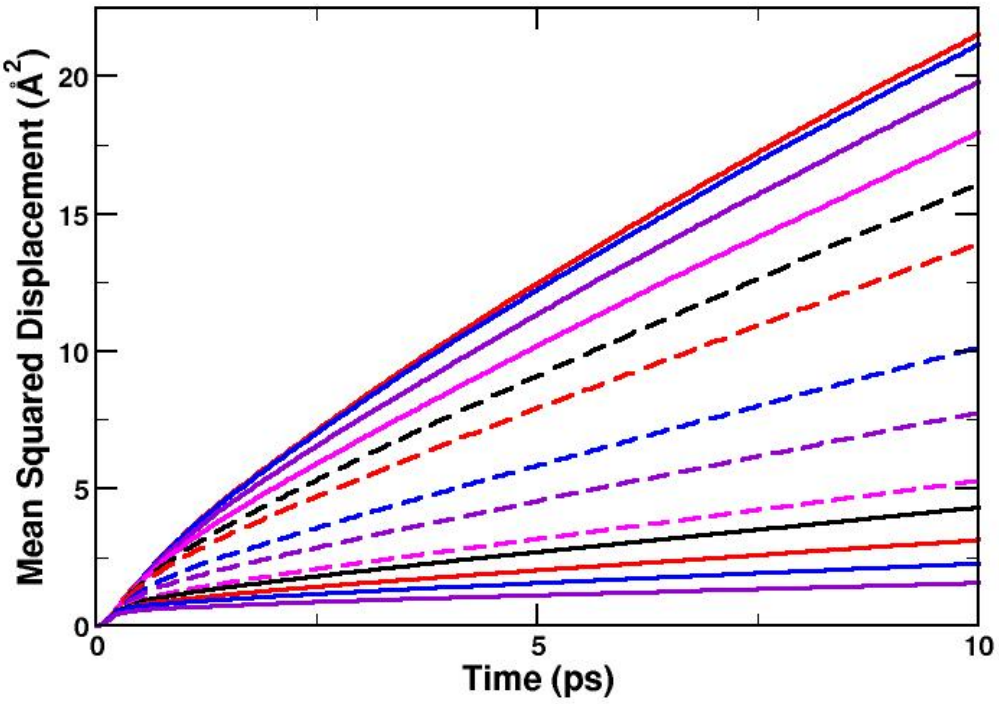


**Figure 3.8** shows the Pore 01 MSD curves from radial layering. The largest-sloped curves are generally closer to the central pore axis. Starting from the axis (larger slopes), the colors are: red, blue, violet, pink, black dashed, red dashed, blue dashed, violet dashed, magenta dashed, black, red, blue, and violet.

The second analysis method for layer separation, by layering according to the nearest pore oxygen is more computationally intensive. It gives slightly different results, and a graph of the curves that result from this analysis can be seen in **Figure 3.9**. A corresponding table again with the diffusion coefficients calculated for each curve is given (**Table 3.4**). The lines of best fit were calculated, as they were before, between two and ten picoseconds of the squared displacement graph.

| Distance from Pore Center (Å) | Linear Fit | | Diffusion Coefficient $\left(\times 10^{-9}\, m^2/s\right)$ | Percent Contribution |
|---|---|---|---|---|
| | Slope | Intercept | | |
| 1-2 | 1.94 | 2.60 | 3.23 | 2.01 |
| 2-3 | 1.89 | 2.59 | 3.15 | 3.16 |
| 3-4 | 1.78 | 2.33 | 2.97 | 4.59 |
| 4-5 | 1.61 | 2.06 | 2.68 | 6.38 |
| 5-6 | 1.44 | 1.85 | 2.40 | 7.78 |
| 6-7 | 1.23 | 1.73 | 2.05 | 8.43 |
| 7-8 | 0.876 | 1.43 | 1.46 | 11.14 |
| 8-9 | 0.656 | 1.25 | 1.09 | 12.68 |
| 9-10 | 0.427 | 1.03 | 0.712 | 14.08 |
| 10-11 | 0.332 | 1.02 | 0.553 | 11.41 |
| 11-12 | 0.226 | 0.888 | 0.377 | 8.28 |
| 12-13 | 0.148 | 0.819 | 0.247 | 4.54 |
| 13-14 | 0.0919 | 0.660 | 0.153 | 3.53 |

**Table 3.3** shows the linear fit values for the MSD function calculated between 2-10 ps for Pore 01 based on layers defined by their closeness to the pore axis with the percent of molecules contributing to each layer.

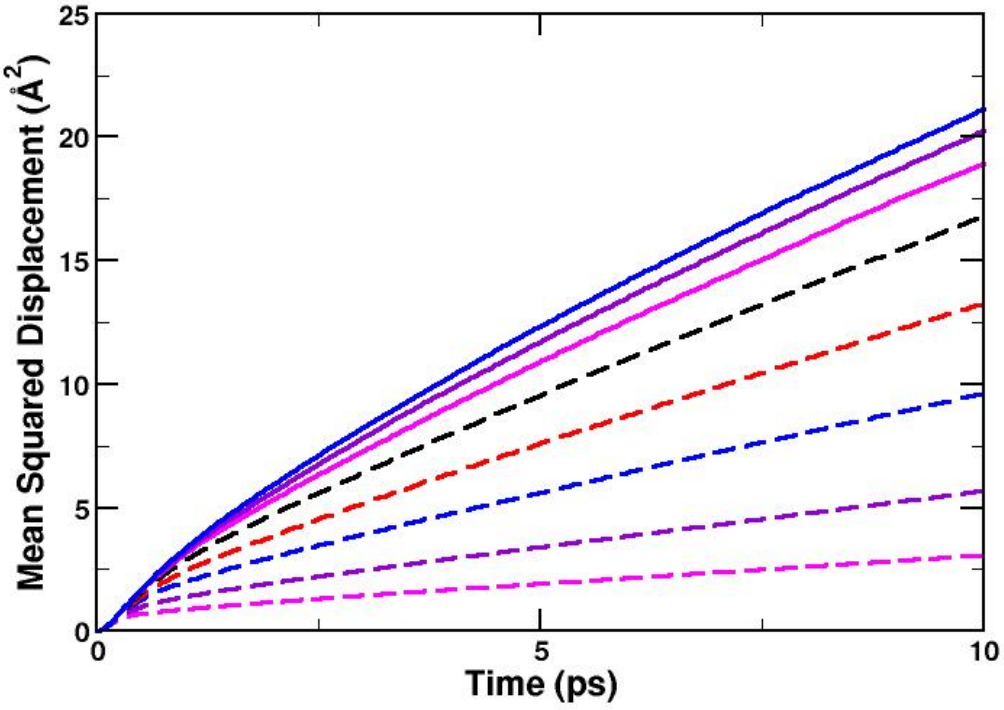


**Figure 3.9** shows the MSD function curves separated according to their closeness to a pore oxygen. The color scheme is thus: dash pink, 1-2 Å; dash violet, 2-3 Å; dash blue, 3-4 Å, dash red, 4-5 Å; dash black, 5-6 Å; solid pink, 6-7 Å; solid violet, 7-8 Å; solid blue, 8-9 Å.

For consistency, **Table 3.4** values also start farthest away from the wall and move toward the pore framework. Fewer layers are present in this analysis because the pore does not necessarily sit directly around the *z*-axis so every molecule is within approximately 10 Å of an oxygen atom even though they may reach as far as 16 Å away from the pore center.

| Distance to Nearest Pore Oxygen (Å) | Linear Fit | | Diffusion Coefficient $\left(\times 10^{-9}\, m^2/s\right)$ | Percent Contribution |
|---|---|---|---|---|
| | Slope | Intercept | | |
| 8-9 | 1.88 | 2.75 | 3.13 | 2.76 |
| 7-8 | 1.80 | 2.52 | 3.00 | 4.90 |
| 6-7 | 1.69 | 2.31 | 2.82 | 5.81 |
| 5-6 | 1.50 | 1.98 | 2.50 | 8.76 |
| 4-5 | 1.17 | 1.70 | 1.95 | 13.1 |
| 3-4 | 0.822 | 1.47 | 1.37 | 13.7 |
| 2-3 | 0.459 | 1.10 | 0.765 | 25.0 |
| 1-2 | 0.234 | 0.743 | 0.390 | 25.4 |

**Table 3.4** lists the diffusion coefficients for $CH_3CN$ molecules separated by layers relative to the nearest pore structure oxygen. It also shows the relative number of molecules in each layer, not normalized for volume.

Combining directional and layering effects leads to the information available in **Figure 3.10** and **Table 3.5**. **Figure 3.10** shows the graph with the corresponding data in **Table 3.5** that represents the diffusion in the *z*-direction only. The same general trend is again seen with the largest slopes belonging to those that are farthest from the pore wall. The *z*-direction diffusion coefficient is consistently higher than the total diffusion coefficients for any given layer. The first inner layer to give a significant and therefore statistically reliable value for the diffusion constant is that between seven and eight angstroms away from an oxygen atom (at 2.76%). The value for the constant is $3.13 \times 10^{-9}\, m^2/s$ when all three dimensions are considered and is $3.83 \times 10^{-9}\, m^2/s$ at the

same distance when considering the *z*-direction only. This is a 22% increase, and the values between the two are tabulated in **Table 3.5**.

| Distance to Nearest Oxygen | Linear Fit | | Diffusion Coefficient $\left(\times 10^{-9}\, m^2/s\right)$ | Percent Increase from 3-D |
|---|---|---|---|---|
| | Slope | Intercept | | |
| 8-9 | 0.765 | 0.806 | 3.83 | 22.4 |
| 7-8 | 0.741 | 0.746 | 3.70 | 23.3 |
| 6-7 | 0.686 | 0.699 | 3.43 | 21.6 |
| 5-6 | 0.600 | 0.644 | 3.00 | 20.0 |
| 4-5 | 0.463 | 0.602 | 2.32 | 19.0 |
| 3-4 | 0.330 | 0.547 | 1.65 | 20.4 |
| 2-3 | 0.184 | 0.416 | 0.918 | 20.0 |
| 1-2 | 0.0932 | 0.278 | 0.466 | 19.5 |

**Table 3.5** shows the diffusion coefficients calculated from the line of best fit between 2-10 ps for each layer relative to the closest pore oxygen in Pore 01. The calculations are for the *z*-direction only and the last column lists the relative increase in diffusion coefficient from three dimensions.

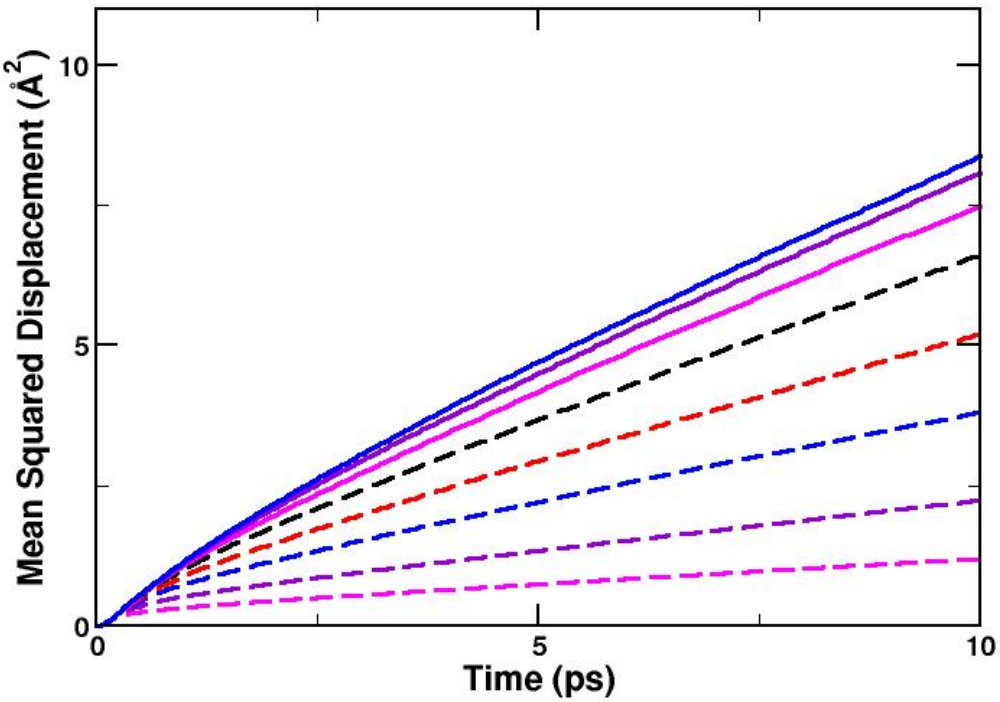


**Figure 3.10** shows the MSD function curves for diffusion in the *z*-direction only by layered by nearest pore oxygen in Pore 01. The pink dashed line represents those molecules within 1-2 Å of an oxygen atom, violet dashed is 2-3Å, blue dashed is 3-4 Å, red dashed is 4-5 Å, black dashed is 5-6 Å, solid pink is 6-7 Å, solid violet is 7-8 Å, solid blue is 8-9 Å, solid red is 9-10 Å, and solid black is 10-11 Å.

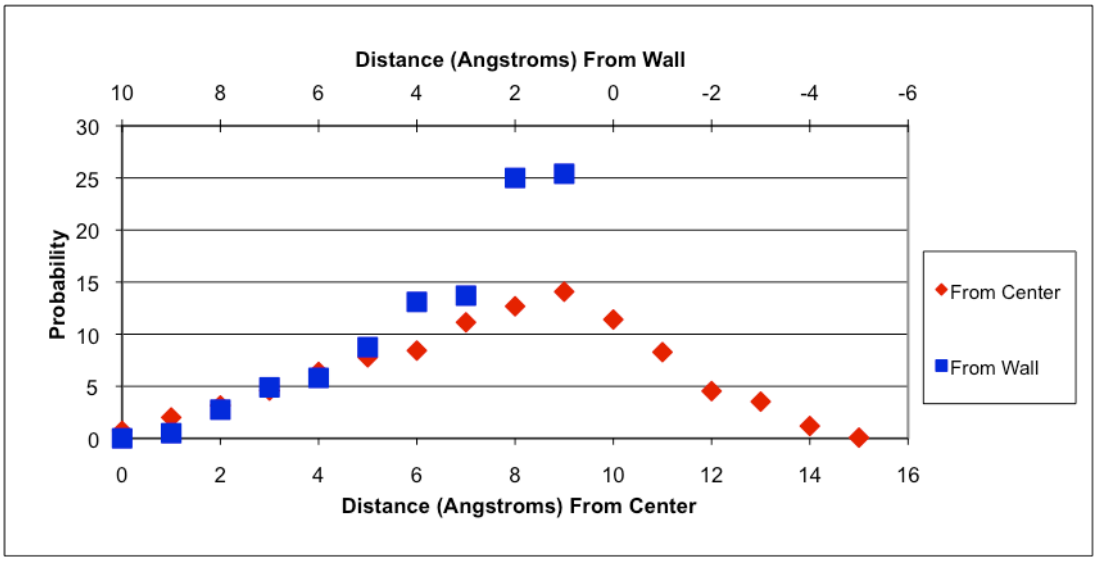


**Figure 3.11** shows a comparison between the two layering methods. The blue squares represent the population of each layer relative to the nearest pore oxygen, with the distance from the nearest oxygen labeled on the upper axis. The red diamonds analogously represent the population of the layers found by their radial distances from the *z*-axis with said distance labeled on the lower horizontal axis.

## 1.3. Pore Charge Effects

The silica pores during the majority of the simulations had charges that caused hydrophilic surface chemistry with hydroxyl-terminated groups protruding into the pore cavity. However, turning off the pore charges can set up a hydrophobic environment so electrostatic effects are eliminated. This was done in order to find molecules that were immobilized in the pore due to static effects (**Figure 3.1**), but a diffusion coefficient comparison was also conducted to better understand the origin of the slower dynamics.

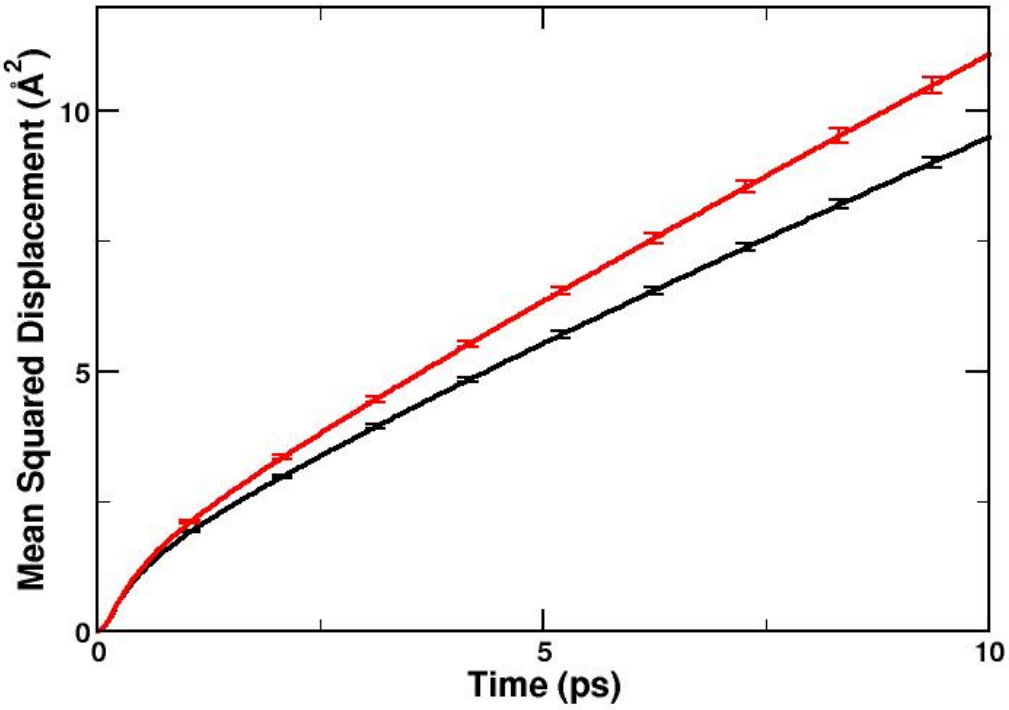


**Figure 3.11** shows the MSD functions for both the charged (black) and uncharged (red) pores.

The overall MSD graph comparing the charged to the uncharged pore is shown in **Figure 3.11**. The red curve is from the non-charged pore. It has the larger slope, and the diffusion coefficient is $1.62(3)\times10^{-9}\,m^2/s$ compared to $1.36(4)\times10^{-9}\,m^2/s$ for the charged pore.

The distribution of these molecules within the neutral pore is of interest relative to the charged pore, and the percent distributions are listed in **Table 3.6**. For comparative purposes, the percent contributions from the original pore are listed again in this table. This information is shown graphically in **Figure 3.12**.

| Distance to Nearest Oxygen (Å) | Diffusion Coefficient $\left(\times 10^{-9}\, m^2/s\right)$ | Percent Contribution, Charged Pore | Percent Contribution, Neutral Pore |
|---|---|---|---|
| 8-9 | 2.75 | 2.76 | 3.02 |
| 7-8 | 2.63 | 4.90 | 5.10 |
| 6-7 | 2.49 | 5.81 | 7.07 |
| 5-6 | 2.32 | 8.76 | 11.0 |
| 4-5 | 2.01 | 13.1 | 11.2 |
| 3-4 | 1.58 | 13.7 | 10.9 |
| 2-3 | 1.15 | 25.0 | 37.5 |
| 1-2 | 1.02 | 25.4 | 13.6 |

**Table 3.6** lists the diffusion coefficients for the uncharged pore according to layering by the nearest pore oxygen. The percent contributions for each layer of the charged and uncharged systems is also listed in the final two columns.

A comparison of the diffusion coefficients by layer is shown in Figure 3.13 and 3.14. The diffusion coefficients were calculated in this manner for the ten charged pores in order to find the size of the error bars. At the time of this writing, the uncharged pore diffusion coefficient had only been calculated for Pore 01, so error bars are excluded. However, the standard deviation of the charged pores' diffusion coefficients ranged from 9.2% to 12.0% when using 10 blocks (each pore was a "block").

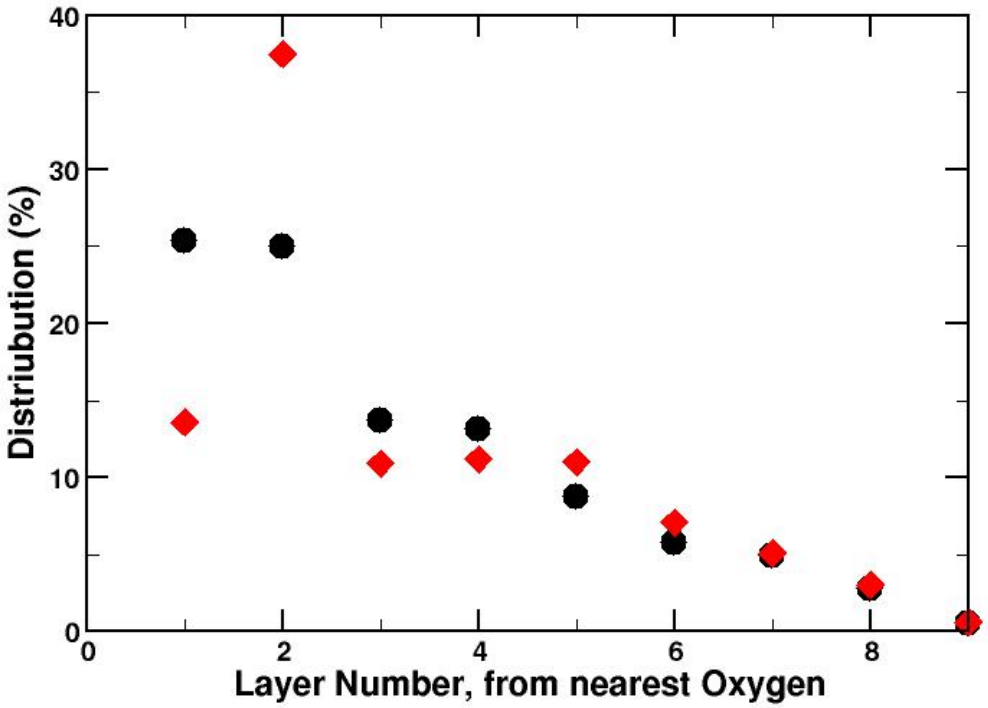


**Figure 3.12** shows a comparison of the average distribution of molecules within Pore 01. The layer number corresponds to the distance in Å of a molecule from the nearest pore oxygen i.e. layer one contains molecules that are 1-2 Å from the nearest oxygen in the pore framework. The black circles represent molecules in the charged pore, the red diamonds are those in the uncharged pore.

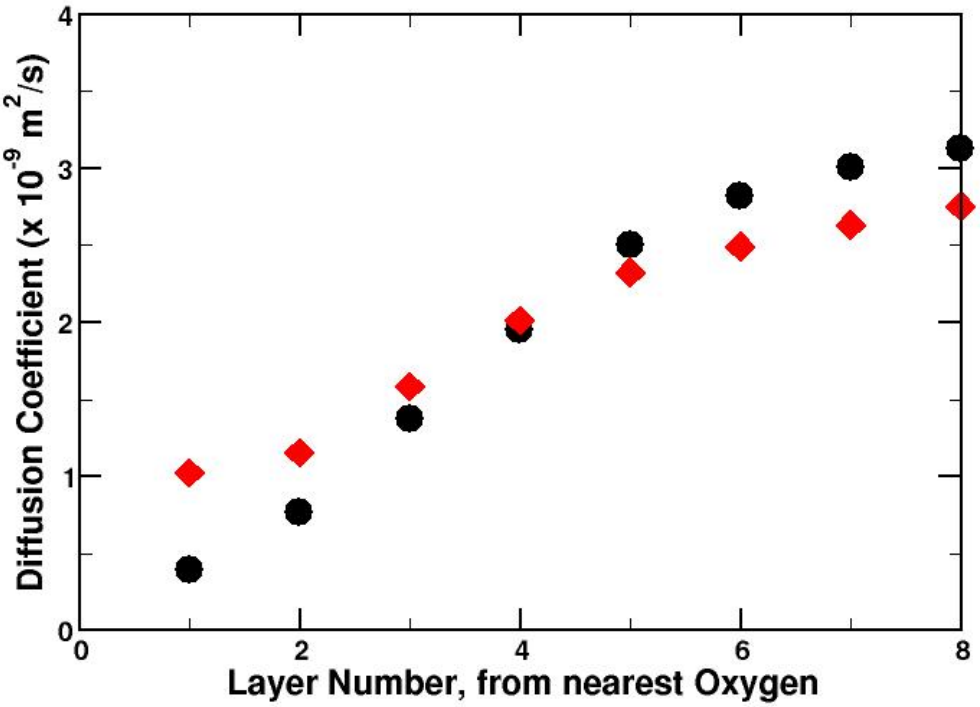

**Figure 3.13** shows the diffusion coefficient for Pore 01 charged (black circle) and uncharged (red diamond) according to where the molecules are within the pore.

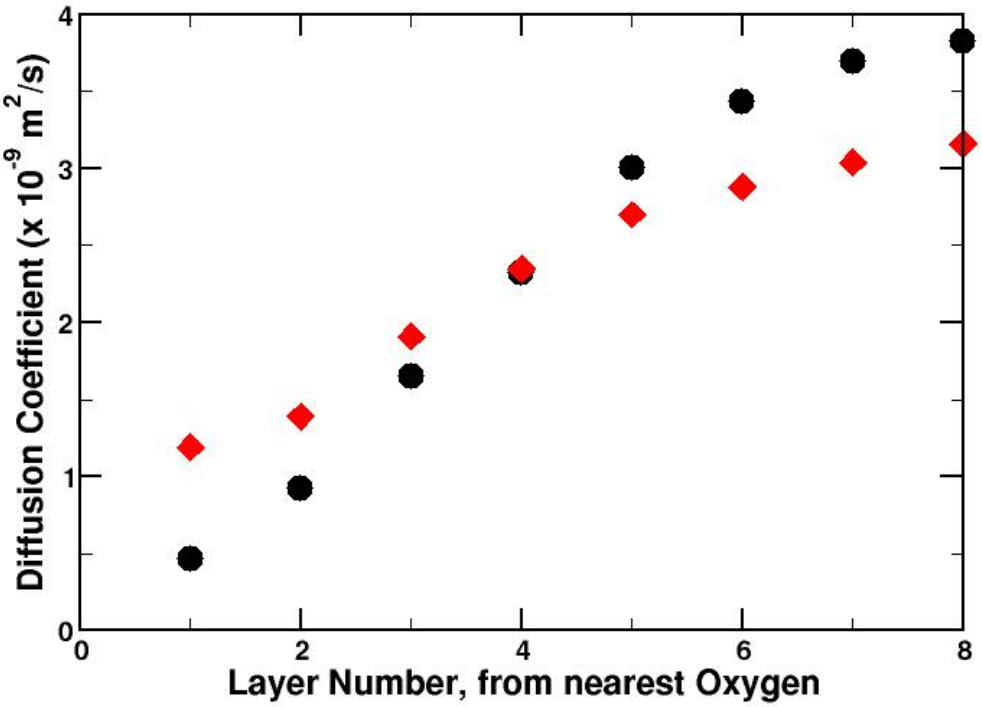


**Figure 3.14** shows the diffusion coefficient in the *z*-direction in Pore 01 when it is charged (black circle) and uncharged (red circle) according to the placement of the molecule within the pore. The layer number corresponds to the distance in Å the molecules are found from the nearest pore oxygen.

## 1.4. Temperature Effects

The effect of temperature can also be studied using the simulations. Trajectories at 275 K and 325 K were used to compare to the results, discussed so far, which are all for 300 K. Bulk liquid trajectories were also run in order to compare the temperature effect to those of the confined system. **Figure 3.15** shows the result of the overall squared displacement when averaged over all of the molecules in the pore. The blue curve represents the lower temperature and the red curve represents the higher temperature. As is apparent by the figure, the slope of the lower temperature curve (taken between two and ten picoseconds) is the smallest meaning the diffusion coefficient is also the smallest of the three. The quantitative values for these slopes are

found in **Table 3.7**. The diffusion coefficients in the fourth column can be compared and are found to have the same absolute increases from the lower temperature to the higher temperature. A similar table to those found above with layer separation is seen in **Table 3.8**. The corresponding figures look very similar to those already shown so they are omitted, but **Table 3.8** should be useful in elucidating some trends. Because the intercepts are not used in calculations of the diffusion coefficient, they are omitted for **Table 3.8**. These values are found using the nearest pore oxygen as the criteria for layering.

| Temperature | Linear Fit | | Diffusion Coefficient $\left(\times 10^{-9}\, m^2/s\right)$ |
|---|---|---|---|
| | Slope | Intercept | |
| 275 K | 0.673 | 1.32 | 1.124(7) |
| 300 K | 0.818 | 1.41 | 1.36(4) |
| 325 K | 0.959 | 1.52 | 1.60(4) |

**Table 3.7** lists the diffusion coefficients calculated from diffusion of molecules in Pore 01, 2-10 ps.

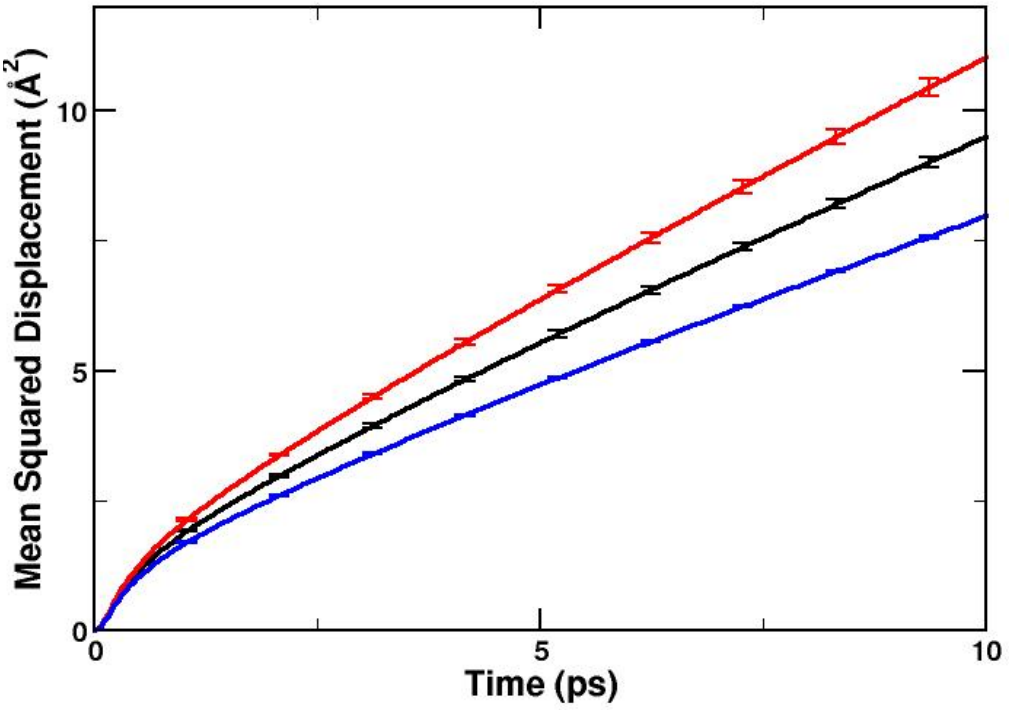


**Figure 3.15** is a graph of the MSD functions for three temperatures: 275 K (blue), 300 K (black) and 325 K (red) inside Pore 01 over all of the molecules.

The higher diffusion coefficient at higher temperature relative to 275 K is independent of placement within the pore. The relative difference does decrease as molecules get farther away from the pore structure. For the closest molecules, the relative increase in diffusion coefficient is 81.8%, while the molecules that are 3$^{rd}$ farthest away have a relative increase of 23.6%. Also, the percent contribution (not corrected for available volume) seems to favor the higher temperature for layers that are not by the wall, while the lower temperature leads to a larger contribution closer to the wall.

| | 275 Kelvin | | | 325 Kelvin | | |
|---|---|---|---|---|---|---|
| Distance to Nearest Oxygen (Å) | Slope | Diffusion Coefficient $\left(\times 10^{-9}\, m^2/s\right)$ | Percent Contribution | Slope | Diffusion Coefficient $\left(\times 10^{-9}\, m^2/s\right)$ | Percent Contribution |
| 8-9 | 1.73 | 2.88 | 2.69 | 2.14 | 3.56 | 2.84 |
| 7-8 | 1.60 | 2.66 | 4.76 | 2.03 | 3.39 | 5.00 |
| 6-7 | 1.46 | 2.43 | 5.68 | 1.87 | 3.12 | 5.98 |
| 5-6 | 1.29 | 2.15 | 8.62 | 1.68 | 2.81 | 8.85 |
| 4-5 | 0.985 | 1.64 | 13.1 | 1.35 | 2.26 | 13.2 |
| 3-4 | 0.663 | 1.11 | 13.8 | 0.979 | 1.63 | 13.7 |
| 2-3 | 0.354 | 0.590 | 25.0 | 0.566 | 0.944 | 25.0 |
| 1-2 | 0.169 | 0.281 | 25.9 | 0.307 | 0.511 | 24.9 |

**Table 3.9** lists the diffusion coefficients by layer within Pore 01 at the 275 K and 325 K calculated from the best-fit lines between 2-10 ps. The percents of the total number of molecules present in each layer are also tabulated.

Temperature effects were also calculated for the bulk system in order to see if temperature has a larger effect in the pore system compared to the bulk. The graph of the bulk MSD is similar to that for the confined system, but is included in **Figure 3.16** for completeness.

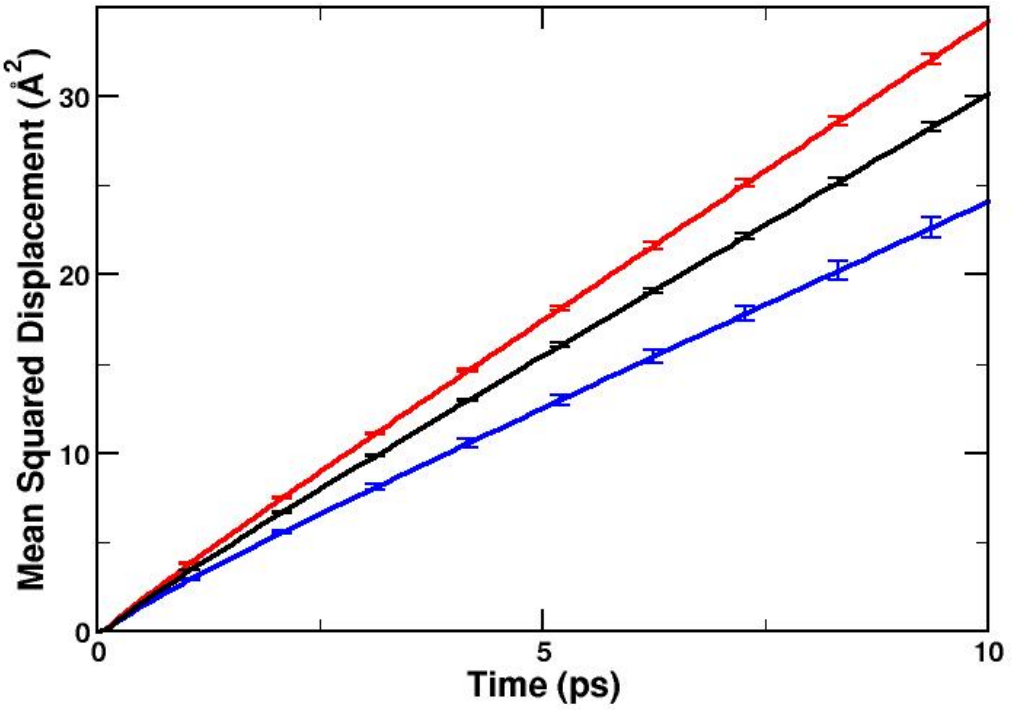


**Figure 3.16** shows the MSD curves at 3 temperatures, 275 K (blue), 300 K (black), and 325 K (red) for bulk liquid acetonitrile.

| Temperature | Linear Fit | | Diffusion Coefficient $\left(\times 10^{-9}\, m^2/s\right)$ |
|---|---|---|---|
| | Slope | Intercept | |
| 275 K | 2.34 | 0.814 | 3.9(2) |
| 300 K | 2.95 | 0.656 | 4.91(8) |
| 325 K | 3.37 | 0.596 | 5.61(9) |

**Table 3.9** lists the diffusion coefficients for the three temperatures in bulk liquid acetonitrile.

## 2. Discussion

### 2.1. Bulk versus Confined

The maximum radial movement looked similar to **Figure 3.1** for all ten pores. That is, the molecules that were not immobilized moved approximately the same distance while those that were immobilized had a distinct dip in the graph. After examining the graphs of all ten pores, 5 Å was chosen to be the cutoff radial change length at which a molecule was deemed immobilized in the pore wall. If it did not move more than 5 Å, then it was 'immobilized'. This value could at first glance seem rather large, but pockets in the pore structure that could hold two $CH_3CN$ molecules allow for some movement but should not be considered part of the system yet can involve radial changes of nearly this magnitude. Two methods are available to calculate the diffusion coefficient. The first is to plot the average squared displacement of the molecules with respect to time. The slope of this curve, assuming it is linear, is equal to $6D$, where $D$ is the diffusion coefficient.

As would be intuitively expected, the slope of the linear part of the mean squared displacement curve of the confined system is much smaller than that of the bulk system. This makes sense; much like people in a crowd on a football field the bulk system molecules can move quite a bit without having to turn around while if the same number of people per unit area are present in a small hallway, they are more likely to need to change their path and have more difficulty removing themselves from their original spots. A better direct comparison of the dynamics utilizes bulk in one dimension compared to pore dynamics in the $z$-direction only. Despite considering only ten-picosecond correlations, undoubtedly molecules would diffuse farther if they were not

confined in two dimensions because of the impossibility of going any farther than approximately 24 angstroms in the *x*- or *y*-directions. Diffusion differences caused indirectly by the confinement are more important in this study.

The shape of the MSD curve is not perfectly linear. A magnified picture of the bulk and confined curves (from **Figure 3.2**) is shown below in **Figure 3.17**. The curves for the bulk and confined systems match each other at short time scales because the movement at those times is inertial. Following Newton's equations of motion, the square displacement is approximately proportional to the square of the time at very small times, so this curve is expected.

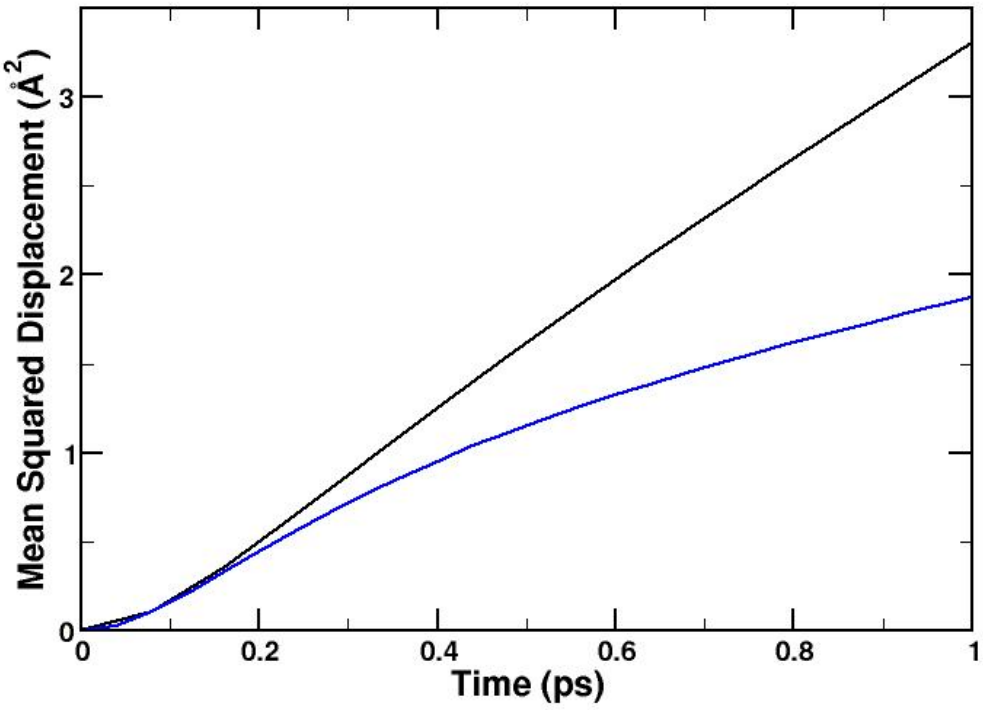


**Figure 3.17** shows the MSD for confined liquid acetonitrile (blue curve) and bulk liquid acetonitrile (black curve), magnified to show details.

The first point calculated for the bulk system is at 0.08 ps. At that point, the curves for the systems actually overlap. This indicates that the occurrence of the same inertial motion is happening. A slight variation begins at the next point, 0.16 ps, and the

two curves diverge from there. The movement that occurs with molecules before they run into anything else—whether it is the pore wall or another molecule—dominates the inertial motion. The inertial movement should be the same and therefore these results corroborating with that is encouraging.

## 2.2. Across the Pores

As seen in **Figure 3.5**, the slopes of the MSD curves across the pores look similar and the quantitative comparison can be made from the values in **Table 3.2**. The smallest diffusion coefficient is found in Pore 08. Pore 08 also has the largest number of silanol moieties (86 – **Table 2.1**). The largest diffusion constant, on the other hand, is in Pore 02, which has 60 silanol groups. The average number of silanol groups across all ten pores is 59 with a standard deviation of 1.2, so Pore 02 has an average number of silanol moieties. Though increasing the number of silanol moieties would seem to decrease diffusion constants within the pores because of electrostatic interactions, this does not appear to be directly the case. The pore with the fewest number of silanols is Pore 10, which has the 4$^{th}$-highest diffusion coefficient. Based on these comparisons, perhaps the correlation of the smallest diffusion constant with the highest number of silanols is coincidental. A more thorough examination of silanol count to diffusion will be continued in the next section when considering layers near the pore surface.

## 2.3. Layers

Both methods for separating the molecules by layers, radially and by nearest pore wall oxygen, were closely examined. Because the former method is less expensive computationally, it was tried initially. The resultant curves (**Figure 3.8**) show some of the problems that are inherent in this method. First, the three curves that represent those

molecules closest to the z-axis overlap. This actually may not be a "problem" and could in fact be that the layers are too small and no difference exists past a certain point in the interior. However, these pores, though when being formed were symmetrically set around the z-axis, are not necessarily perfectly centered on it at their current state, and from this data it is unclear whether the layers close to the z-axis are in fact those that are furthest from a wall. If they were, a conclusion that pore wall effects are minimized by the time the inner 3 Å are reached can be made. The volume of these inner layers is also quite small ($\pi r^2 h$, r = 1, 2 and 3 Å) so the statistics are not as well characterized. A further indication of this is the percent contribution of each of the three curves. The total contribution from all three is 5.89% meaning a total of about nine molecules gave the results in the figure so very little can be said with certainty of the inner curves except that the calculated diffusion coefficient is still smaller than that in the bulk system.

Once the initial three curves are passed, a steady trend in the diffusion coefficients is seen until the last two layers. As the layers considered move away from the pore center, the diffusion constant decreases. This decrease makes sense because pore wall effects would be expected to increase as a molecule is closer to the wall. The wall effects also are expected to slow acetonitrile molecules because of steric hindrance and because the hydrophilic head groups would theoretically interact favorably with polar $CH_3CN$.

After the perfect correlation between layer and diffusion constant for the eleven layers, the coefficients again move away from this trend. In the two outer-most layers, the diffusion coefficient first increases to higher than the both of the previous two layers and the final layer is still larger than the final coefficient in the layers that follow the

trend of decreasing coefficient as the layer moves away from the center. Again, inspection of the percent contribution can give an indication of the problem. The total input between these two layers is 1.27% that would indicate approximately two molecules contributing to both. With this relatively small data set, no conclusions can be made about these two curves and their diffusion constants. However, this problem exposed the need for a different analysis. Presumably, these two final curves are next to the wall, and therefore should be averaged in with 'wall' molecules rather than thrown out. They do contribute useful data even if that data cannot statistically stand alone.

The next method for separating molecules into layers was to find the nearest pore oxygen to any given molecule and calculate the distance between the two. That distance governed the layer to which a molecule belonged. Despite having a higher computational cost, circumventing the aforementioned problem of not knowing where a molecule is relative to the pore is worthwhile. Upon inspecting **Figure 3.9**, one can see the curve representing the molecules farthest away from the pore surface is not as straight as the other given curves. Not surprisingly, then, the percent contribution is low for this – a mere 0.0086% or well less than one molecule. Drawing any conclusions from this curve would be meaningless. The next-closest curve is the red one that does look like the others with a relatively straight slope, but it also has a contribution of slightly less than one molecule so it also does not yield a reliable calculated diffusion coefficient, though as can be seen in **Table 3.4**, they do both follow the general trends. The rest of the layers each have a large enough contribution to give relevant results. The trend in this case is that as a molecule is closer to the pore wall, it diffuses more slowly. This is obvious from the diffusion coefficients given in **Table 3.4**, and unlike in the

previous analysis, it is true across every layer. The results then seem more reasonable. Molecules closest to the pore surface have a diffusion coefficient of $0.390 \times 10^{-9}\ m^2/s$, nearly ten times slower than layers farther away from the wall. The wall seems to have a large contribution to the dynamics of solvent molecules.

After some consideration, the thought that these values may be more from steric hindrance rather than solvent-pore interaction was considered. A simple yet effective way to test this theory was to calculate diffusion coefficients in the *z*-direction only. This direction has periodic boundary conditions and molecules are free to move in it. The calculated diffusion coefficients are tabulated in **Table 3.5**. The first row of data, that which represents molecules that are 7-8 Å away from the pore wall, shows the calculated coefficient as $3.83 \times 10^{-9}\ m^2/s$. This value is 22% higher than the corresponding coefficient when all three dimensions are considered. For the eight statistically significant layers, the *z*-direction diffusion coefficient is larger than the corresponding coefficient. Obviously, the presence of the pore that stops the molecules from moving the *x*- or *y*-directions does have an effect on the diffusion coefficient. However, the relative values within the layers are about the same. That is, when comparing layer 7-8 to 0-1 in three dimensions, the diffusion coefficient decreases by 87.5%, and doing the same comparison in the *z*-direction values only, the diffusion coefficient decreases by 87.8%. By these numbers, the pore wall seems to affect the *z*-direction diffusion in a similar fashion to the *x*- or *y*-direction diffusion. This conclusion is reinforced visually by a comparison between **Figure 3.10** and **Figure 3.9**. Though **Figure 3.10** has a higher total square displacement, the graphs look similar otherwise.

## 2.4. Pore Charge Effects

Because this current effort is focused on confinement and the effect of the pore wall on solvent dynamics, the simple question of how the pore charge in particular affects diffusion and placement of the molecules within the confined system was asked. As can be seen in **Figure 3.11**, turning the charges of the pore wall off—in other words, making them hydrophobic—does change the displacement. The molecules move more quickly when in the hydrophobic pore relative to the hydrophilic pore. This result is not surprising since the $CH_3CN$ molecules are expected to interact favorably with the hydrophilic surface. The diffusion coefficient is not the only difference between the two systems.

A second question was asked regarding the placement of the molecules within the pore. As would be expected, the largest number of molecules in the hydrophilic pore is found in the layer closest to the wall. The molecules are attracted to the pore surface and the largest volume is also found there. This is not true for the neutral pore. With the charges off and a hydrophobic surface exposed, the polar acetonitrile molecules do not get as close to the pore wall as their charged-wall counterparts. The layer within 1 Å of the wall contains substantially fewer molecules in the neutral pore than in the charged pore. Conversely, the next layer contains substantially more. The percent decrease and increase from the charged pore to the neutral pore are 46.5% and 50.0%, respectively. The neutral pore seems to establish more definite layers as can be seen by the inconsistent percent contributions despite steady increases in volume as layers near the pore surface. This may be due to layering cutoffs that just happen by chance to show this in the neutral pore even though it also could exist for the charged pore.

The smoothness of the change in diffusion coefficients in both charged and uncharged pores according to the layer to which the molecules belong (**Figures 3.13** and **3.14**) would make it seem as if a conclusive difference exists. However, until further analyses to calculate error in the neutral pore are complete, conclusions may not be drawn. Currently, error bars have been calculated for the charged pore, and if the error is similar in the uncharged pore, then deductions regarding a difference between the two when considering that layers will not be possible.

## 2.5. Temperature Effects

The final analysis for the diffusion coefficient was to inspect temperature effects. This is clearly not a "pore effect", however, differences caused by changing temperature are potentially interesting, both within the pore and when compared relative to the bulk system. They tell us about the activated nature of diffusion, e.g. the barriers involved. The initial test was to simply look at the overall displacement differences among the three temperatures. These values are shown in **Table 3.7**, and the absolute change in diffusion coefficient from the 275 K to 300 K and from 300 K to 325 K are the same. The relative change of the diffusion coefficient is larger from the coolest temperature, but it is not currently believed that this is due to any pore effect.

The next information considered was what happened to the layers when the temperature changed. The breakdown of the layers stayed fairly constant, with a slightly higher affinity for the cooler molecules to reside next to the pore surface indicating attraction to the surface. A more interesting observation was the relative difference in diffusion coefficient from the wall-layer to inner-layer between the two temperatures. At 275 K, the relative decrease is 90.2% from the 7-8 layer to the 0-1 layer while at 325

the relative decrease is 85.6% between the same two layers. This would indicate that at the cooler temperature, the $CH_3CN$ molecules "feel" the wall more strongly next to the surface or "feel" it less than the warmer system when closer to the interior, or a combination of the two. The former point would seem to be more likely because of the slower diffusions; the cooler acetonitrile can be friendlier with the wall than their warmer counterparts. The direct comparison between these two values confirms the difference – the relative increase from 275 K to 325 K nearest the pore wall is 81.8% while in layer 7-8 the relative increase is only 23.6%.

In order to check the relative differences caused by temperature between the bulk and confined systems, the bulk trajectories were analyzed. The graph of the results and the calculated values can be seen in **Figure 3.14** and **Table 3.9**. Visual inspection of **Figure 3.16** shows that the graph is similar to **Figure 3.15** in that the largest-sloped curve is the red that represents the highest temperature followed by the middle-temperature black curve and then the lowest-temperature blue curve. Perhaps more interesting is the relative differences with temperature when compared to the confined system. The percent increase of the diffusion coefficient between 275 K and 300 K in the bulk system is 26.2% and is 14.2% between 300 K and 325 K. These same comparisons for the confined system yield 21.4% and 17.6%, respectively. Obviously, the lower temperature affects the bulk system more than the confined system and the higher temperature affects the confined system more than the bulk. At this point, the reason for this is unclear.

# Chapter 4: Reorientational Correlation Times

Reorientational correlation times are an important piece of molecular dynamics information. The speeds of reactions depend upon molecules interacting in favorable way, physically. Solvation dynamics are governed by reorientation times, and a transition state's stability is affected by the orientation of solvent molecules. Each molecular dynamics simulation described in Chapter 2 was analyzed to obtain a reorientational autocorrelation function in order to characterize the reorientational dynamics. This is typically done in terms of the time scales for decay of the autocorrelation function. The curve fitting for these correlation functions in the confined system is complex, and many methods were undertaken in order to find the best possible description of the reorientational dynamics.

## 1. Results

### 1.1. Bulk versus Confined

As was done for diffusion, the initial test for the reorientational correlation function, $C_l(t) = \langle P_l(\vec{e}(t) \bullet \vec{e}(0)) \rangle$ (see **Eq. 2.4**), was to calculate it using the bulk system. After that was completed, the same calculation was performed for the confined pores. The resultants are shown in **Figure 4.1** for $l = 1$, i.e., $C_1(t) = \langle \vec{e}(t) \bullet \vec{e}(0) \rangle$ (simply $x$ for **Eq. 2.4**). The black curve underneath the red represents the bulk autocorrelation function while the blue corresponds to the confined system (arbitrarily in pore 01). The red curve is the biexponential best-fit curve (**Eq. 4.1**) which gives the timescale $\tau_1$=3.03 ps for reorientation of acetonitrile in the bulk liquid. A biexponential graph is used to

account for the small inertial component at very short times, and the best fit equations were restricted to ensure the exponent's coefficients (*I* and *R* in **Eq. 4.1**) summed to 1.0. As can be seen visually, this curve matches the experimental curve well, and quantitatively, it has a correlation coefficient of 0.999985. That correlation time, $\tau_1$, can then be compared to the accepted experimental and/or simulation values to check for validity. **Figure 4.2** shows the curves from the reorientational correlation function using the 2nd-order Legendre polynomial. This is the correlation function when $P_l$ in **Eq. 2.4** is equal to $P_2 = \frac{1}{2}\left(3x^2 - 1\right)$ so the biexponential fit to the bulk curve (again shown in red) yields the value for $\tau_2$. The form of the biexponential function is:

$$C_l(t) = I * \exp(-t/\tau_l) + R * \exp(-t/\tau_l) \qquad (4.1)$$

where *I* is the weight of the inertial component, $\tau_I$ is the inertial time, *R* is the weight of the reorientation time component, and $\tau_l$ is the reorientational correlation time using the $l^{th}$-order Legendre polynomial.

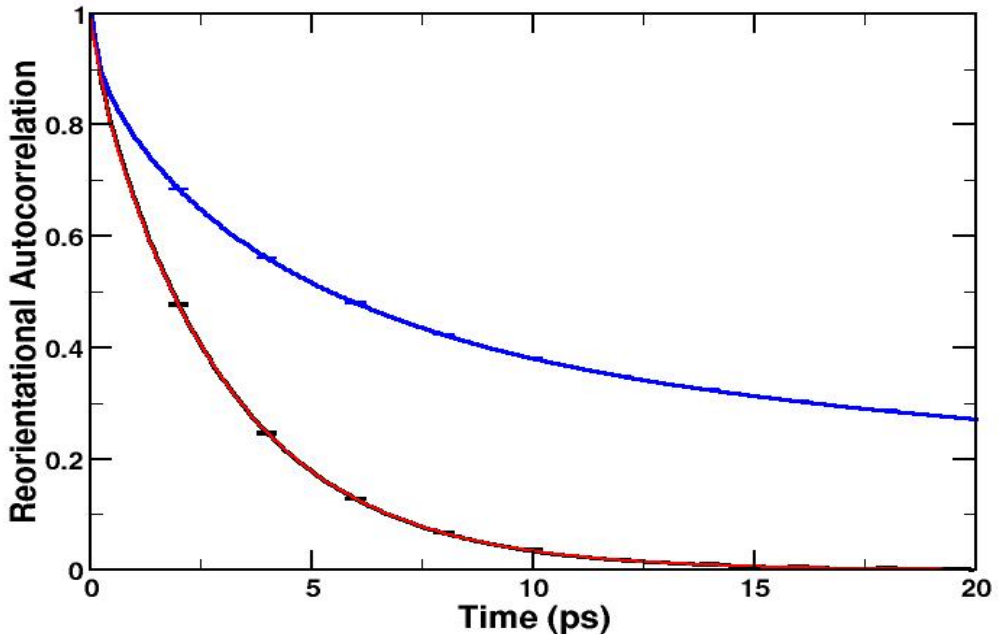


**Figure 4.1** shows the reorientational correlation functions, $C_1(t)$, for bulk liquid acetonitrile (black curve) with its best-fit curve superimposed in red and for confined liquid acetonitrile (blue) in Pore 01. These curves are made using the 1st Legendre polynomial for $P_l(t)$ in **Eq. 2.4**.

Both of these figures are meant to show bulk information more than confined. Clearly, the confined curves have not come close to approaching zero in this time 20 ps frame, but the bulk curves have.

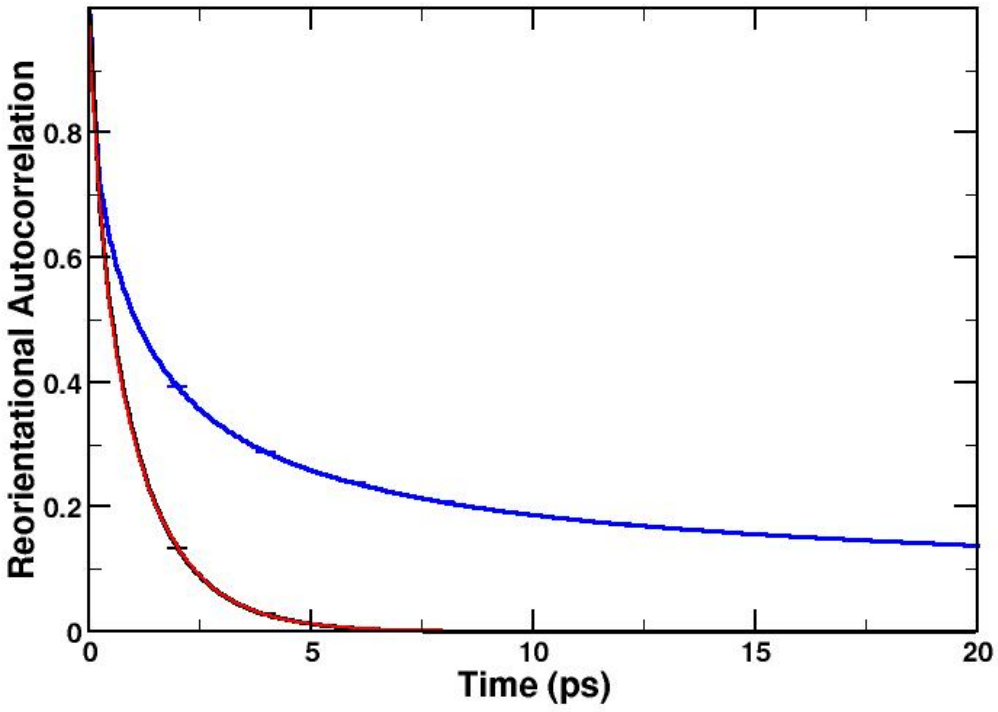


**Figure 4.2** shows the reorientational correlation curves, $C_2(t)$, for bulk (black) and confined (blue) liquid acetonitrile. These curves utilize the 2nd Legendre polynomial for $P_l(t)$ in **Eq. 2.4**. The red curve is the best-fit curve for bulk liquid $CH_3CN$.

| Polynomial Order | Inertial Weight, $I$ | Inertial Time, $\tau_I$ (ps) | Reorientation Weight, $R$ | Reorientation Time, $\tau_l$ (ps) |
|---|---|---|---|---|
| 1 | 0.08 (2) | 0.32 (9) | 0.92 (2) | 3.03 (9) |
| 2 | 0.30 (2) | 0.28 (2) | 0.70 (2) | 1.22 (3) |

**Table 4.1** lists the inertial and reorientational correlation times and weights for bulk liquid $CH_3CN$. Polynomial order refers to which Legendre polynomial they utilize. Both were fit using a bi-exponential function (**Eq. 4.1**). Numbers in parentheses indicate one standard deviation in the final digits from 20 blocks.

In **Table 4.1**, an inertial time with a smaller weight of the curve is recorded with the calculated reorientation time for these trajectories. The calculated value can then be compared to previously obtained (via experiment or theory) literature values given in **Table 4.2**. In principle, the $\tau_1$ obtained from the present simulations should agree with the ANL values in **Table 4.2**. That they do not suggests a potential error in the calculations of Reference 10. The present $\tau_1$ are in reasonable agreement with the measured values, differing by 8.3% and 40.1% for $\tau_1$ and 16.4% for $\tau_2$.

| Constant | Edwards[19] | Jorgensen[20] | Guardia[21] | ANL[15] | Experiment |
|---|---|---|---|---|---|
| $\tau_1$ (ps) | 1.91 | 1.28 | 1.34 | 1.93 | 3.28[22], 3.68[23] |
| $\tau_2$ (ps) | 0.82 | 0.61 | 0.58 | 0.80 | 1.02[24] |

**Table 4.2** lists the previously calculated theoretical and experimental values for the reorientational correlation times.

## 1.2. Pore Heterogeneity

### 1.2.1. Across the Pores

Reorientational correlation functions were also calculated for each of the ten silica pores. The graph of these curves is shown in **Figure 4.3**. Like the MSD curves, the reorientational correlation graphs are not identical but do not differ dramatically. Again the solid black line represents the Pore 01 molecules that will be used for further confined analyses in this chapter. Though more analyses will be explored in later sections, these curves were fit to tri-exponential decay functions, and the reorientational correlation times using that method for each pore are presented in **Table 4.3**.

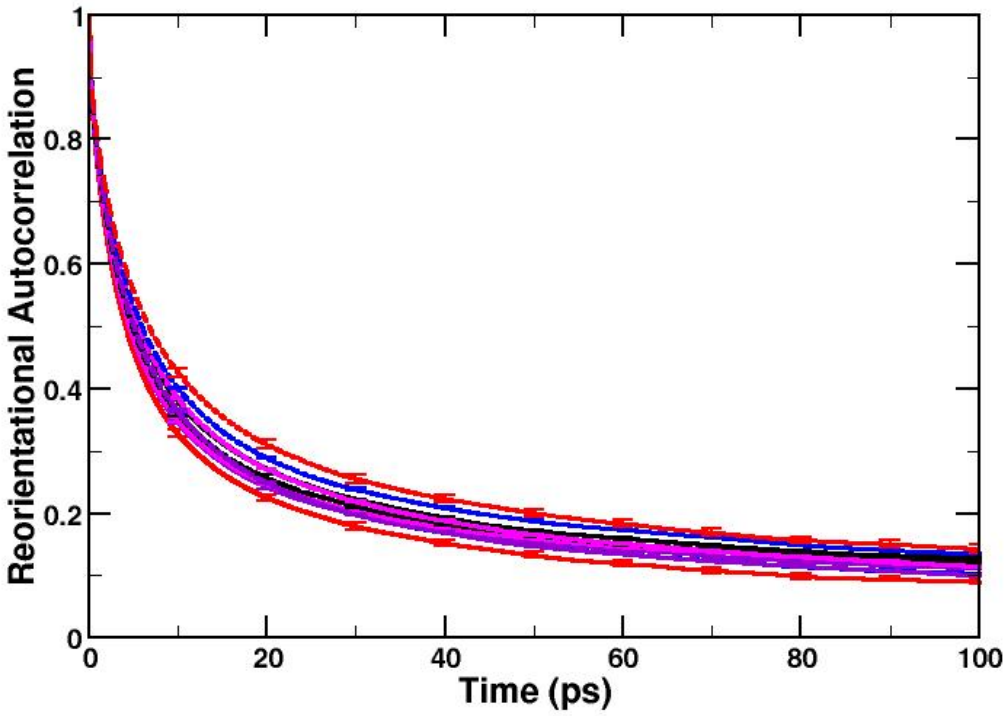


**Figure 4.3** shows the reorientational correlation functions for the 10 pores, ~12 Å radius. The color scheme is as follows: Pore 01, solid black; 02, solid red; 03, solid blue; 04, solid violet; 05, solid pink; 06, dashed black; 07, dashed pink; 08, dashed blue; 09, dashed violet; 10, dashed red. The curves were calculated using $P_1$ in **Eq. 2.4**.

### 1.2.2. Layers

In a similar fashion to the layer differences seen for the MSD curves, the dynamics of reorientation also varies depending on the position of a given molecule. Again, the correlation functions were first calculated as a function of distance from the center of the pore. The resultant curves using the first order Legendre polynomial are shown in **Figure 4.4**. Of course, the number of molecules within each of these curves is the same as was true for the MSD layers (chapter 3), and the values for the tri-exponential fit can be found in **Table 4.4**.

| Pore | Weight 1 | Time 1(ps) | Weight 2 | Time 2 (ps) | Weight 3 | Time 3 (ps) |
|---|---|---|---|---|---|---|
| 01 | 0.28(2) | 1.2(1) | 0.48(1) | 9.1(8) | 0.25(1) | 136(8) |
| 02 | 0.28(3) | 1.0(1) | 0.46(2) | 9(1) | 0.26(2) | 120(20) |
| 03 | 0.26(3) | 1.0(2) | 0.49(2) | 7(3) | 0.25(2) | 110(10) |
| 04 | 0.28(3) | 1.1(2) | 0.47(3) | 8.7(9) | 0.26(2) | 140(20) |
| 05 | 0.27(2) | 1.1(1) | 0.48(2) | 8.6(9) | 0.25(2) | 140(40) |
| 06 | 0.27(5) | 1.1(3) | 0.46(3) | 10(2) | 0.27(2) | 150(20) |
| 07 | 0.26(3) | 1.1(2) | 0.48(2) | 9(1) | 0.26(2) | 110(20) |
| 08 | 0.24(2) | 1.0(2) | 0.48(3) | 9.4(7) | 0.28(2) | 150(20) |
| 09 | 0.27(5) | 1.1(3) | 0.49(3) | 9(2) | 0.24(3) | 130(40) |
| 10 | 0.27(4) | 1.1(2) | 0.48(3) | 8.5(9) | 0.25(2) | 100.(20) |
| Average | | 1.11 | | 8.7 | | 120 |
| Std. Dev. | | 0.07 | | .4 | | 10 |

**Table 4.3** lists the reorientational correlation times for tri-exponential fits for the ten pores. These were fit to curves that were correlated to 100 ps. The numbers in parentheses are the errors calculated by one standard deviation using eight blocks.

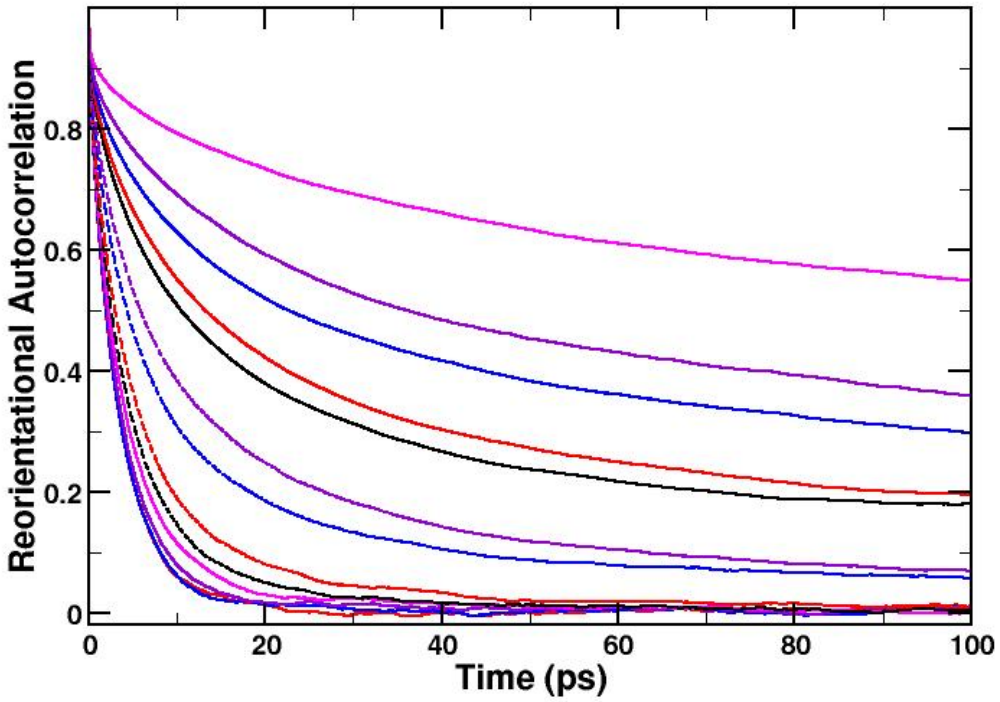


**Figure 4.4** shows the 1st Legendre polynomial reorientational correlation functions layered radially in Pore 01. Starting from the *z*-axis, the steepest curves, the coloring is as follows (1 Å widths): red (0-1 Å), blue (1-2 Å), violet (2-3 Å), magenta (3-4 Å), black dash (4-5 Å), red dash (5-6 Å), blue dash, (7-8 Å) violet dash (8-9 Å), magenta dash (9-10 Å), black (10-11 Å), red (11-12 Å), blue (12-13 Å), violet (13-14 Å), magenta (14-15 Å) – the last are those that have the gentlest-sloping curves at small (<10 ps) times.

The curves that represent those molecules that are closest to the center axis around which the pore was originally created are those that are the steepest at short times. The general trend of these curves is that those that are closest to the *z*-axis have the quickest drop to $C_1$=0. As the slopes become less extreme, the overall curve flattens, and they represent the molecules farther away from the center axis.

Another component of the graph is that the first six curves – those representing the molecules that begin their correlations within 6 Å of the *z*-axis – have reached a zero correlation value within approximately 50 ps while the molecules in the other layers are still correlated to their initial orientations.

To further investigate the position dependence, the layers were studied according to their placement relative to the pore wall rather than the *z*-axis. These curves can be seen in **Figure 4.5** and are also calculated using the first-order Legendre polynomial.

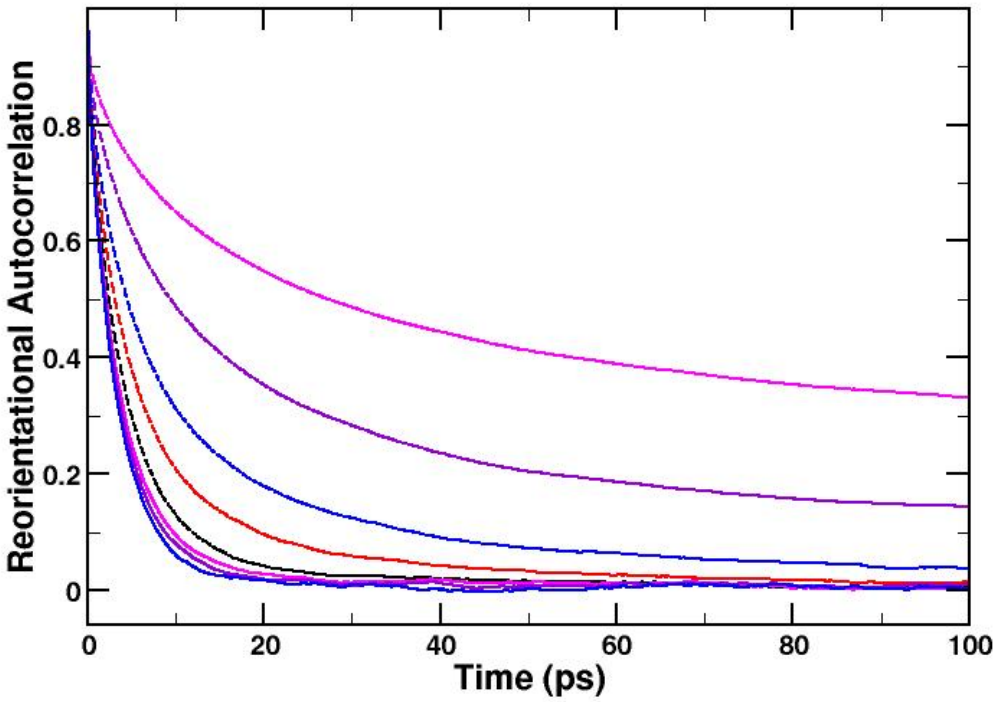


**Figure 4.5** shows reorientational correlation functions from the 1st Legendre polynomial in Pore 01 using the nearest pore oxygen atom for layering standards. Starting farthest from the pore wall, the colors are: blue (8-9 Å from pore wall), violet (7-8 Å), pink (6-7 Å), black dash (5-6 Å), red dash (4-5 Å), blue dash (3-4 Å), violet dash (2-3 Å) and pink dash (1-2 Å). The final curves are those with the gentlest slopes at small (<10 ps) times.

The curves in **Figure 4.5** are similarly represented as those in **Figure 4.4**. Those curves that have the steepest initial slopes are farthest away from the wall while those with the gentler slopes are closest to the pore wall. The number of molecules per layer is the same here as the layered distribution when calculating the MSD in Chapter 3 (**Table 3.4**).

Both **Figure 4.4** and **Figure 4.5** clearly show that molecules either farther from the *z*-axis or next to the pore wall are still correlated to their initial orientations after 100 ps. In an attempt to resolve longer time scales, extended trajectories of 20 ns were

carried out. Using the 20 ns trajectory data, reorientational correlation curves for the layers and for the average of all of the molecules, sans the structurally immobilized, were plotted. The graphs showing this information are shown in **Figures 4.6** and **4.7**. The plots are of correlation functions based on the 1st Legendre polynomial.

The main characteristic of note in these figures is that the correlation curve does not reach zero for the overall average, and the layers show that as well for the two curves closest to the pore wall. The layers are again calculated relative to the nearest pore oxygen and have 1-Å widths. Fitting these curves to a meaningful equation is the next important step. First, a tri-exponential fit was tried with the results both over all the molecules and by layer shown in **Table 4.4**.

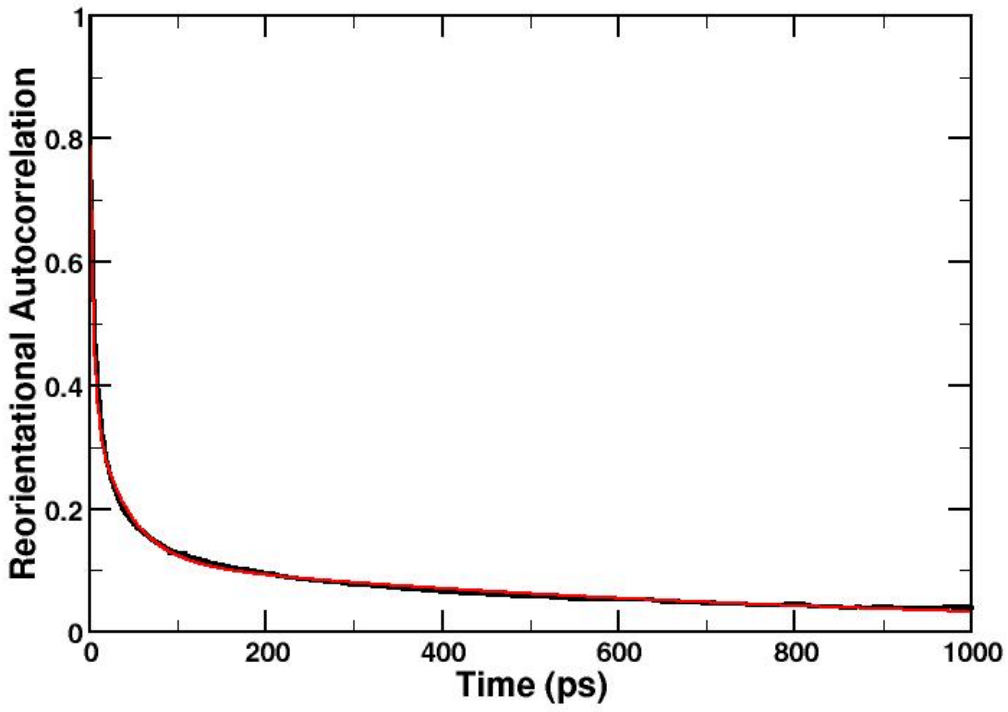


**Figure 4.6** is the reorientational correlation function over all of the molecules in Pore 01 using the 1st Legendre polynomial (black) with a best-fit curve (red).

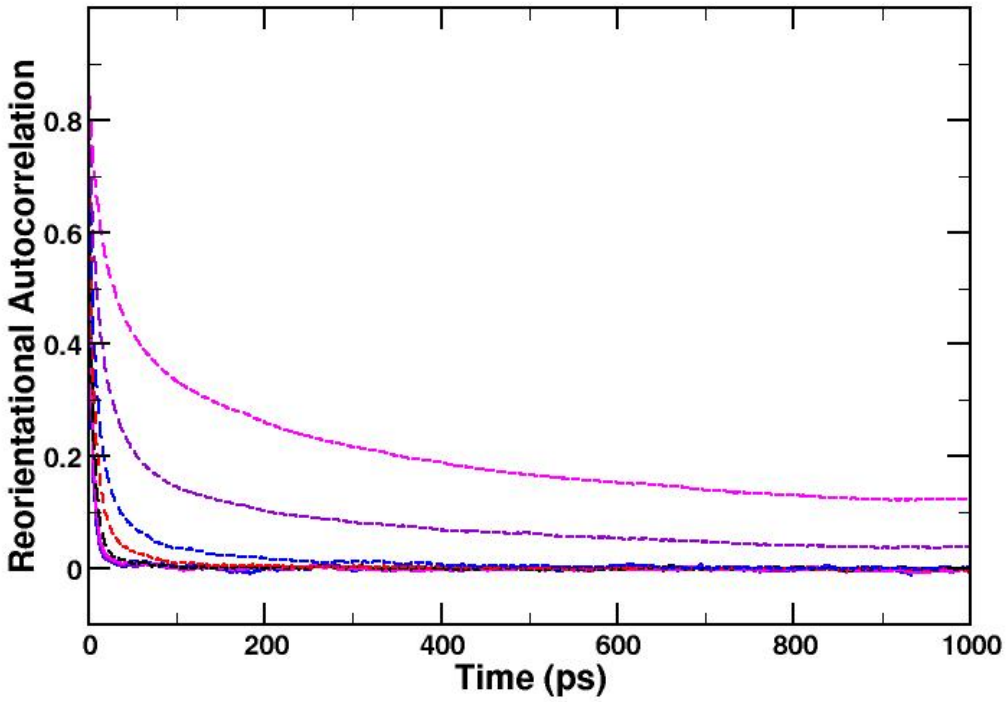


**Figure 4.7** shows the layered reorientational correlation functions. From closest to the edge, the colors are: pink dash, violet dash, blue dash, red dash, black dash, pink, violet, and blue

| Curve | Weight 1 | Time 1 (ps) | Weight 2 | Time 2 (ps) | Weight 3 | Time 3 (ps) |
|---|---|---|---|---|---|---|
| Total | .61 (4) | 3.6 (4) | .27 (2) | 38 (9) | .12 (2) | 800 (300) |
| 7-8 Å | 0.199 | 0.733 | 0.781 | 3.88 | 0.020 | 48.3 |
| 6-7 Å | 0.208 | 0.668 | 0.761 | 4.20 | 0.031 | 41.1 |
| 5-6 Å | 0.258 | 0.900 | 0.698 | 5.08 | 0.044 | 38.5 |
| 4-5 Å | 0.349 | 1.34 | 0.587 | 7.80 | 0.064 | 66.0 |
| 3-4 Å | 0.449 | 2.21 | 0.479 | 14.6 | 0.072 | 160. |
| 2-3 Å | 0.485 | 4.27 | 0.379 | 35.5 | 0.136 | 668 |
| 1-2 Å | 0.440 | 7.69 | 0.303 | 96.2 | 0.257 | 1210 |

**Table 4.4** lists the reorientational correlation times for tri-exponential curve fits over all of the molecules ("Total") and by layer. The distance from the nearest pore oxygen is listed in column 1, rows 3-9. These values were calculated using 1000 ps correlation times.

After completing these calculations, some trends can be seen in the data. First, at distances farthest from the pore wall, a relatively short time scale is resolvable. As the layers move closer to the pore surface, the short time scale increases to the same order of magnitude as what was the 2nd time scale and the 2nd time scale closer to the wall is similar to the 3rd when farther from the wall. The longest time scale gives a less than 10% contribution to the total for all of the layers except the two closest to the pore wall; in fact, this contribution nearly doubles between the 3-4 Å layer and the 2-3 Å layer and again between the 2-3 Å and 1-2 Å layers. The final time scale of the layer closest to the wall is longer than is reliable because it is beyond the range of the graph.

Each of the layers needs a reliable best-fit curve, but based on these calculations, the curves at different areas of the pore need to be treated differently due to their differing time scales – an extra time scale seems to "grow in" as the layers approach the pore wall. Also, the trend shown in **Table 4.4** is that the layers have slow increases or decreases in time scales so a cut-off between pore-wall acting molecules and inner-pore molecules does not exist. To see this graphically, $\log(C_l(t))$ was plotted with respect to time and is shown in **Figure 4.8**. If the time scales are separable, the curve should be piecewise linear.

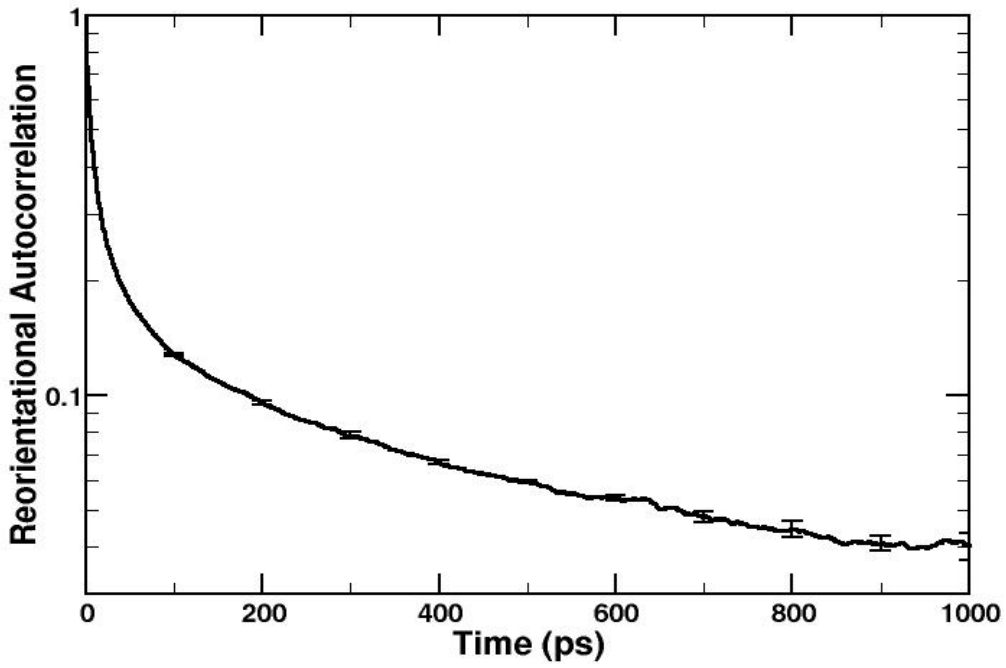


**Figure 4.8** shows the natural log of the reorientational correlation function as a function of time. The original function was calculated using the 1st Legendre polynomial and is in Pore 01.

The curve does not seem to show conclusive evidence of separable time scales because it is nowhere linear. As a result, a stretched-exponential fit (**Eq. 4.2**) was tried using the five layers closest to the wall and the curve representing all of the non-stationary molecules. The five layers were chosen because the values of the correlation function are greater than zero for the majority of the correlation so the stretched exponential curve is defined for those curves.

As can be seen in **Figures 4.9** and **4.10**, the curves are not quite linear. If they did behave like a stretched exponential, then these figures should show a linear trend. As it is, for the overall correlation (**Figure 4.9**) and for the curves not directly against the wall in **Figure 4.10**, two distinct slopes appear. The curves in this case are a result of a stretched exponential analysis that is of the general form:

$$C_l(t) = \exp\left[-\left(\frac{t}{\tau_l}\right)^{\beta}\right] \qquad (4.2)$$

This equation is then manipulated algebraically to yield the form:

$$\log(-\log(C_l(t))) = \beta\log(t) - \beta\log(\tau_l) \qquad (4.3)$$

and when the data is plotted with dependent variable log(-log($C_l(t)$)) versus log($t$), a straight-line fit yields the unknown values: $\beta$ is the slope, and the intercept is $-\beta\log(\tau_l)$. The curves shown in **Figures 4.9** and **4.10** utilize this information. The log($x$) functions in these cases are all considered to be the natural logarithm, and the original curves used were those that had been calculated to 1 ns for previous correlations.

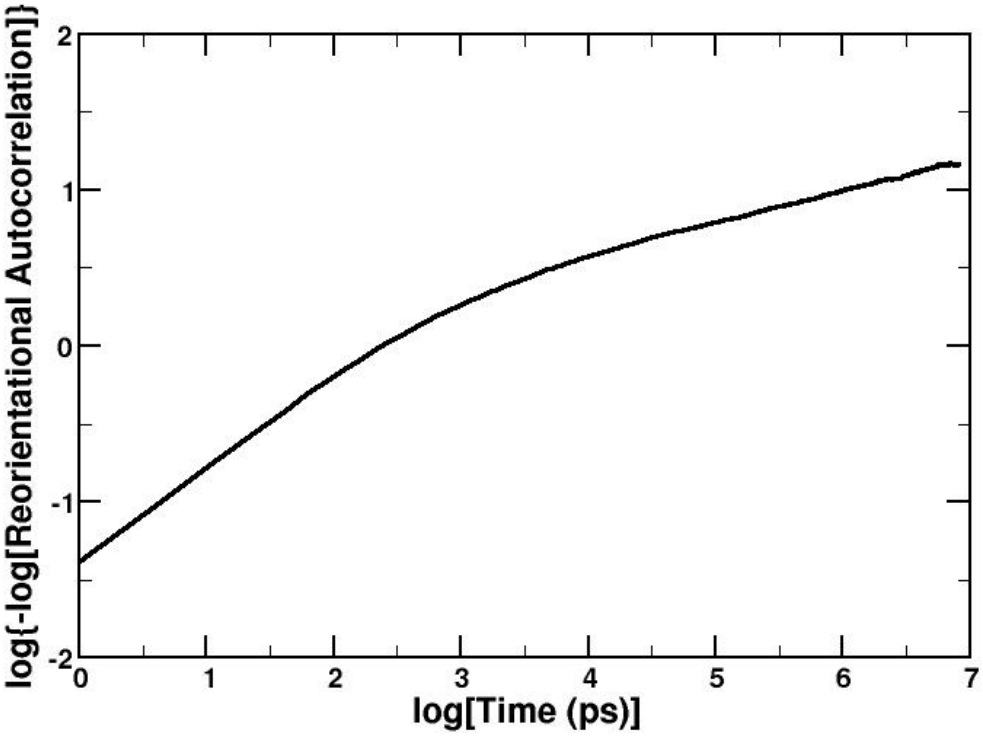


**Figure 4.9** is the stretched exponential curve for all of the mobile molecules in Pore 01. The original correlation was calculated using the 1st Legendre polynomial, and the "log" signifies the natural logarithm function.

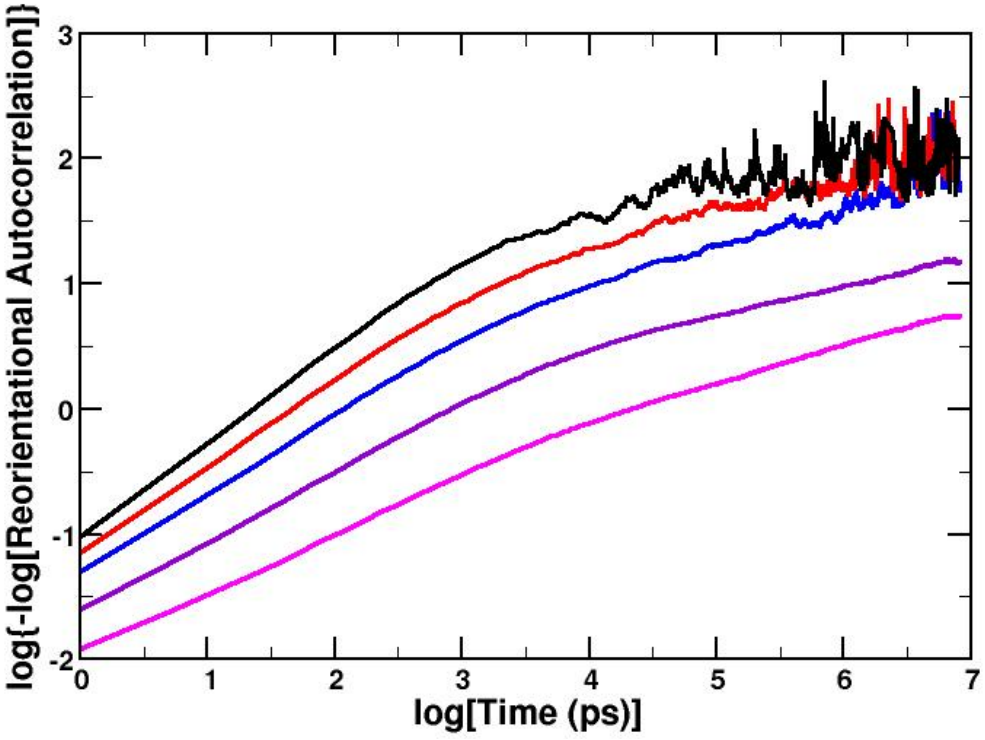


**Figure 4.10** is the stretched exponential curves for the five layers closest to the pore wall. From closest to the wall to farthest away, the colors are: pink, violet, blue, red and black.

| Curve | Slope, short time (β) | Intercept, Short Time | $\tau_1$ | Slope, Long Time (β) | Intercept, Long Time | $\tau_1$ |
|---|---|---|---|---|---|---|
| All Molecules | 0.579 | -1.36 | 10.5 | 0.204 | -0.228 | 3.06 |
| 5-6 Å | 0.749 | -1.02 | 3.90 | 0.0915 | 1.33 | $2.05 \times 10^6$ |
| 4-5 Å | 0.667 | -1.15 | 5.61 | 0.221 | 0.479 | 8.74 |
| 3-4 Å | 0.634 | -1.31 | 7.90 | 0.345 | -0.439 | 3.57 |
| 2-3 Å | 0.558 | -1.62 | 18.2 | 0.240 | -0.461 | 6.83 |
| 1-2 Å | 0.466 | -1.94 | 64.3 | 0.297 | -1.27 | 72.0 |

**Table 4.5** lists the linear fits and resultant reorientational correlation times. The short time was fit to the curves at less than log($t$) = 2.5, and the long time was fit to the curves at greater than log($t$) = 4. The first column's numbers show the distance, in Å, of the molecules represented by that curve to the nearest pore oxygen.

As can be seen in **Figure 4.10**, the curves begin to lose the bent shape as they approach the pore wall with the final (pink) curve, that is next to the wall, nearly completely void of any change in its derivative. The slopes of these curves were calculated, both at the steeper slope at short times (less than log($t$) = 2.5, $t \leq 12$ ps) and at the gentler sloping longer time ranges (greater than log($t$) = 4, $t \geq 55$ ps). This was also completed for the curve representing all of the molecules and the results are shown in **Table 4.5**. The only three curves that would be "reliable" are the two curves representing the molecules closest to the pore wall and the curve that represents all of the molecules because the others have points at which the original function was less than zero and is therefore undefined. Even so, the values for $\tau_1$ do not seem to offer insight to the dynamics of the solvent. After this analysis was completed, one more attempt at a multi-exponential curve fit was undertaken, this time with a tetra-exponential fit. The times for the curves closer to the pore wall matched more closely to the other curves, however, the meaning of a tetra-exponential fit is unclear, and thus the fits are excluded from this document.

### 1.3. Pore Charge Effects

As was done for the mean squared displacement, calculations were completed for the reorientational correlation in completely uncharged pores. The need for it in these analyses is even more important due to the reorientational correlation function never reaching zero for the charged pores. At this point, the cause for the reorientational vector to be correlated to its original vector after a nanosecond is unknown, but theoretically it must be due to either steric or electrostatic interactions. If the reorientational correlation function reaches zero for the uncharged pore, then the

previously stated correlation in the charged pores must be due to charge-charge effects. If the uncharged pore does not reach zero, then the molecules must be sterically hindered in some way that prevents them from reorienting.

The calculations were performed averaging over all the molecules, seen in **Figure 4.11**. Obviously, even after only 100 ps, the molecules have nearly entirely lost their correlation to their initial vector values (shown by the autocorrelation function reaching zero), and the charged pore correlation curve is shown for comparison. The reorientation times are listed in **Table 4.6** along with the values found by using the reorientational correlation layered curves. A tri-exponential curve fit was used to find the values in **Table 4.6**.

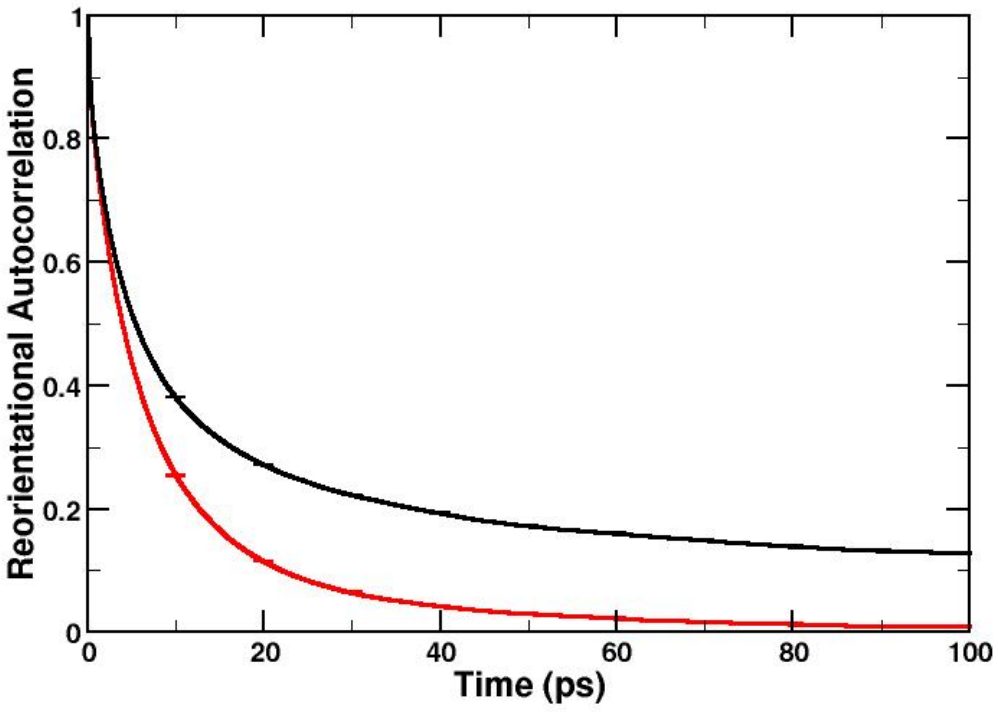


**Figure 4.11** shows the reorientational correlation curves (1st Legendre polynomial) for the charged (black) and uncharged (red) pore molecules. These were both calculated using Pore 01 mobile molecules.

For completeness and comparison, this evaluation was also completed for the pore layers (defined by the nearest pore oxygen). The autocorrelation function for the layers was completed out to 1 ns, and the resultant graph is shown in **Figure 4.12.** The 1 ns graph shows that all of the correlation curves, independent of pore placement, are essentially zero by the end of the trajectory, and the next **Figure 4.13** more clearly shows the values at shorter times.

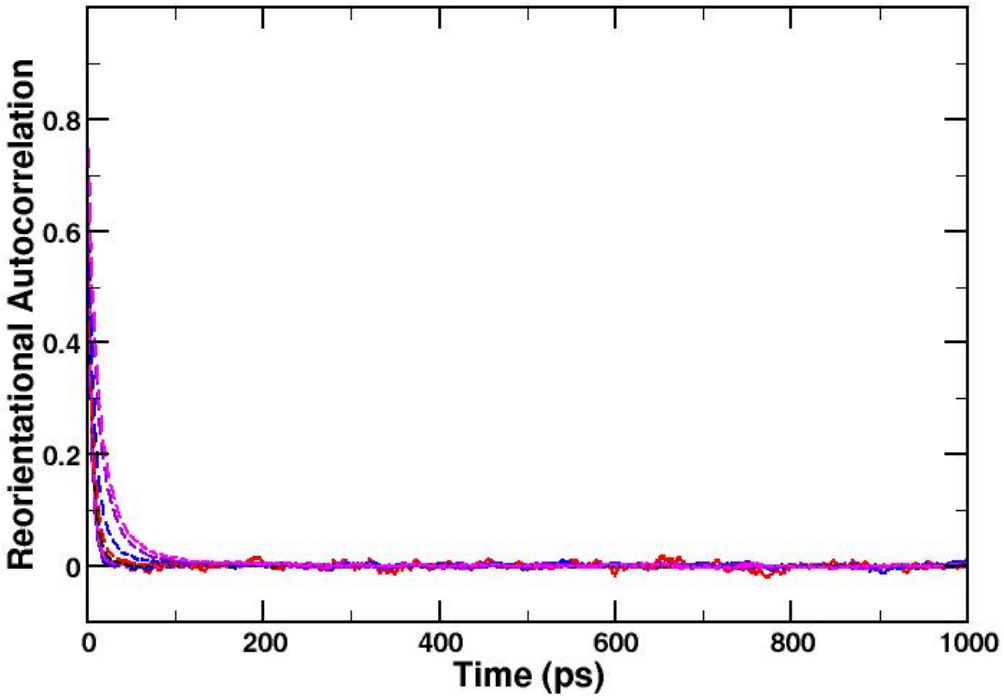


**Figure 4.12** shows the layered reorientational correlation functions for the uncharged Pore 01, 1st Legendre polynomial. They are layered according to the nearest pore oxygen, and are colored from the closest layer: pink dash, violet dash, blue dash, red dash, black dash, pink, violet, blue, red and black.

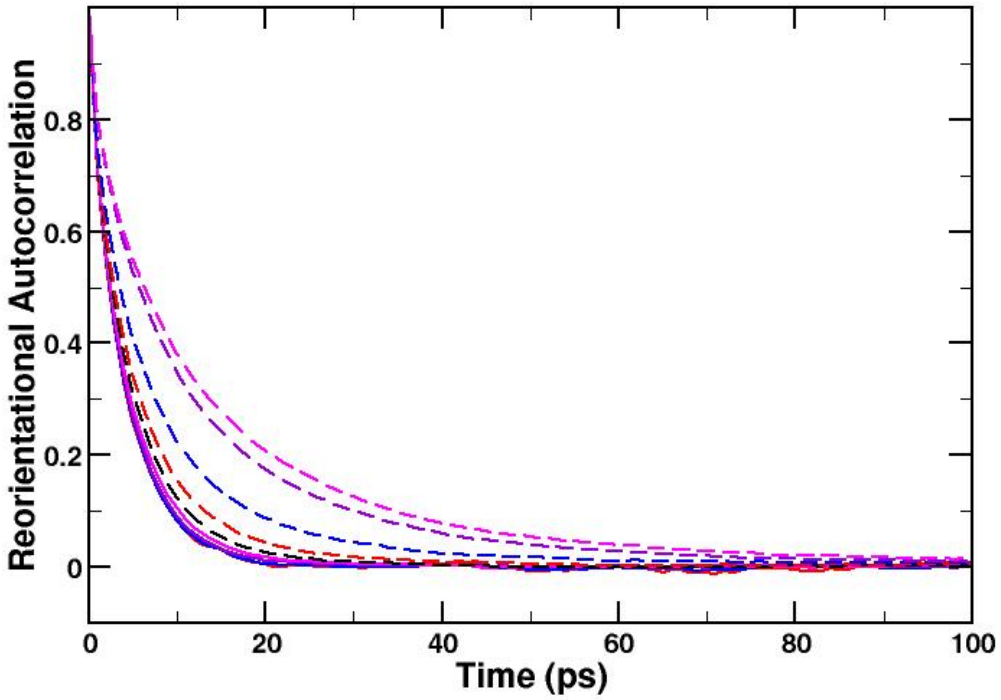


**Figure 4.13** shows a magnification of **Figure 4.12**, the reorientation correlation of the layers defined by the nearest pore oxygen in an uncharged pore.

Both **Figure 4.12** and **4.13** omit the curve that is farthest from the pore wall due to the small number of molecules that contribute to its calculation; the number of molecules in the farthest layer is close to the same as the charged pore (see **Table 3.6** in the previous chapter). The curves for the neutral pore follow the trends perfectly graphically—those that have the sharpest initial decrease are farthest from the pore wall while those that decrease less rapidly are next to the wall.

As for the charged pores, some trends are clearly seen in the data presented in **Table 4.6**. This time, for each of the nine layers shown, a short time scale of around 1 ps is present. A mid-sized time scale that is on the order of several picoseconds is observed, and finally a longer time scale on the order of tens to hundreds of picoseconds is found. The longer time scale has an anomalous trend with layers that are

farther from the pore wall. However, the weight of these time scales is less than 10% for all but the two curves representing those molecules closest to the pore wall.

| Curve | Weight 1 | Time 1 (ps) | Weight 2 | Time 2 (ps) | Weight 3 | Time 3 (ps) |
|---|---|---|---|---|---|---|
| All | 0.17(3) | 0.6(2) | 0.66(4) | 6.4(5) | 0.17(5) | 32(7) |
| 8-9 Å | 0.128 | 0.512 | 0.834 | 4.12 | 0.038 | 7.32 |
| 7-8 Å | 0.155 | 0.653 | 0.843 | 4.43 | 0.002 | 600. |
| 6-7 Å | 0.183 | 0.781 | 0.813 | 4.78 | 0.004 | 168 |
| 5-6 Å | 0.199 | 0.902 | 0.796 | 5.33 | 0.005 | 136 |
| 4-5 Å | 0.253 | 1.10 | 0.736 | 6.28 | 0.011 | 109 |
| 3-4 Å | 0.249 | 1.00 | 0.705 | 7.70 | 0.046 | 53.4 |
| 2-3 Å | 0.185 | 0.899 | 0.656 | 9.67 | 0.159 | 35.1 |
| 1-2 Å | 0.225 | 1.12 | 0.666 | 12.5 | 0.109 | 52.1 |

**Table 4.6** lists the reorientational correlation times using a tri-exponential best-fit curve for all of the molecules in Pore 01 ("All") or layered according to nearest pore oxygen with the distance in Å listed in column 1 for the other rows. The pore is uncharged for these molecules. The numbers in parentheses for row 2 are one standard deviation using eight blocks.

## 2. Discussion

### 2.1. Bulk versus Confined

When comparing the bulk information to the confined, one would expect to see some differences. At the very least, steric hindrance from the pore wall would lead to a decrease in the speed at which a molecule rotates in space. This is an inherent bias, and the curves in **Figures 4.1** and **4.2** show the divergence between the two. Because the curves represented by the confined systems do not decay as quickly, they show that the molecule orientations are correlated to their original positions much longer than bulk

molecules. When compared to experimental values, the correlation times for the bulk liquid are relatively closer than previously performed simulations.

The values obtained for the bulk liquid were less than 0.5 ps for the inertial time scales and 3.03(9) and 1.22(3) ps for the 1st and 2nd Legendre polynomials correlation functions respectively. The calculated value is within 25% of that determined by Fourkas *et al.* (1.64 ps at 293 K and 1.42 ps at 307 K, and the value at 300 K was taken to be the average of these two reported values).[25]

## 2.2. Pore Heterogeneity

### 2.2.1. Across the Pores

The reorientational correlation analysis was performed for each of the ten charged pores. As was seen for the MSD values, the variation across the pores was minimal, with relative standard deviations for the reorientational correlation times ranging from 4-9%. When analyzed using a tri-exponential function for the line of best fit, each had a short time scale close to 1 ps, a mid-range time scale of around 10 ps and finally a longer time scale of over 100 ps. These analyses were all performed using the date in **Figure 4.3**, so the final time scale is unreliable due to it extending past the longest time calculated for the correlation function. After concluding that the general trends for the reorientational correlation times are the same for all of the pores, Pore 01 was used for the other analyses because the same general trend would be observed in the other pores as was seen in Pore 01.

### 2.2.2. Layers

As might be expected, the placement of the molecule within the pore greatly impacts its reorientational correlation curve shapes. For the majority of the layers, using the distance from the *z*-axis as the criteria for separation, the faster reorientation times are those found nearest the *z*-axis, i.e., further from the surface. This is apparent in **Figure 4.4** from the curves that decrease rapidly from their starting point relative to the other curves. That is, the faster the curve decreases to zero, the more quickly the molecules represented by that curve are reorienting in space. The trend for this data that shows the faster reorientation when farther from the pore surface makes sense because the molecule-wall interaction is limited. The density is also less in the center of the pore which can be seen by the nonlinear layering distribution shown in **Figure 3.11**. The only effect from the pore wall for those molecules a few layers away will be what those molecules feel through the intervening molecules. The movement of the molecules in the center is regulated partially by the molecules surrounding them. Much like if a person is in the middle of a crowded room, he or she may not directly feel the effect of relatively stationary people near the wall ("wall flowers"), but the people next to the wallflowers move more slowly than those who are not so a region exists with higher order more closes to the wall, and the gradual changes in slope indicate that the order level of the molecules slowly changes radially. Because some models separate molecules based on specific criteria, more effort was put forth to find a possible line at which the molecules changed their properties according to their placement within the pore structure.

To this end, the pore was first separated into layers defined by their radial distances from the pore center. The graph showing the reorientational autocorrelation functions for the layers is shown in **Figure 4.4**. Two curves were omitted due to the small number of molecules that contributed to the calculation of the curves. However, the two curves are there, and they should be included with any other data analysis for molecules found in the "same" layer relative to the source of the heterogeneity. Since the pore wall effect is the principle source of confinement behavior, these two curves that represent molecules closest to the wall should be included with other molecules that are next to the wall. This led to the realization that though radially defining the layers is computationally less expensive, the data returned is not as reliable and therefore is not as valuable.

To correct for this problem, the other method for layer separation was used and the resultant correlation function curves are shown in **Figure 4.5**. In this case, the curves that represent the molecules considered to be next to the wall are much more reliable both due to their better statistics and the means by which they were defined, measuring distance from the pore surface. Once this analysis was verified, it was then used for the subsequent analyses.

Because the previously completed analyses across all of the pores (**Table 4.3**) showed a long time scale of greater than 100 ps, a longer correlation was tested and the result is shown in **Figure 4.6**. This curve was correlated to 1 ns, and even at this relatively long time scale, some of the molecules retained some correlation to their original value. In order to discover which molecules were responsible—or rather which layers contributed to this correlation—the layered correlation was repeated for the long

time scale, and the results are displayed in **Figure 4.7**. As far as reorientational correlation curves usually go, this is a relatively well-behaved set in that the placement of the molecules directly relates to the decay of the reorientational correlation function.

Upon further inspection of the tri-exponential curve fit values, definite time scales are difficult to determine. However, the layers of the molecules that are far away from the pore wall show a short time scale, presumably due to inertial motion, that is less than 1 ps. This smallest time scale begins to grow, as does the weight of it until next to the pore wall the smallest time scale, at 7.69 ps, is larger than the middle time scales of the farthest five curves. A similar trend of increasing weights is seen in the longest time scale where inner molecules, that act more bulk-like, have very small contribution from it—below ten percent for the long time scale until the curve that is the second-closest to the pore wall surface. This may indicate that the long time-scale is due to pore wall effects such as electrostatic interaction or sterics. The last two curves' time scales seem to indicate that they have four reorientational times of interest because they must have the time scale that is due to inertial movement that is missing in the best fit calculations. To inspect the possibility of separable time scales visually the plot shown in **Figure 4.8** was created. By taking the natural logarithm of the reorientational autocorrelation, the slope at a given time should be $-1/\tau_l$ if it is in fact separable. Various sections of the curve were analyzed, but linear fits were inconclusive.

As previously stated, fitting a curve to four time scales begins to lean toward overkill of analysis, and at present the meaning of even three time scales is not trivial so assigning physical meaning to four time scales is unreasonable. The thought that the confined molecules displayed glass-like behavior was examined next, and a stretched

exponential fit was probed as a possible descriptor. The value for β in **Eq. 4.2** is indicative of how stretched the autocorrelation curve is from its regular exponential decay. The smaller it is, the more "stretched" the function. The values for $\beta$ in for these curves was approximately 0.5 for short times and 0.27 at long times. Because the graphing program available does not fit curves to stretched exponentials, some algebraic rearranging was completed to yield **Eq. 4.3.** The rearranged equation was used to find the line of best fit of the resultant curves. The higher times should be those from the longer time scales, but the numbers are completely unreliable for three of the curves because they were calculated by taking the natural logarithm of a value less than zero and are therefore undefined in areas. The original reorientational autocorrelation curves had effectively reached zero by the time of interest in the stretched exponential plot and as a result have noisy regions. The other curves—those covering all of the molecules and the two closest to the pore wall—give values that are not long relative to the long time scale seen in the tri-exponential fit, and because the molecules definitely have some correlation even after a nanosecond, the stretched exponential was found to be inadequate.

### 2.2.3. Pore Charge Effects

Not knowing the origin of the long time scales led to the analysis of uncharged pores. If the molecules no longer have the long time scales when in the neutral pores, then those times must be due, at least partially, to electrostatic interactions with the pore wall. **Figure 4.11** clearly shows a much faster drop to zero for the curve representing the neutral pore molecules. As would be expected, the reorientation time is faster for the uncharged pores since no electrostatic interactions occur, and this graph shows that they

are completely uncorrelated by 100 ps. The electrostatic pore-liquid interactions are the cause of the extra-long time scales. To see if there is still a large difference among the layers that would be due to sterics only, the layers were analyzed again.

Because long time scales were present in the charged pore, a fit to include them was initiated for the neutral pore, but upon inspection of the graph shown in **Figure 4.12** the thought was abandoned. All of the curves had reached zero by 100 ps as shown in the magnification of **Figure 4.12**, **Figure 4.13**. The position of the molecules does contribute to some dynamics changes even in the neutral pore. However, the longest time scale calculated is around 50 ps. Compared to the long time scales in the hydrophilic pores, this 50 ps reorientational time is small. The other curves that have very small (less than 5%) contributions to the long time scale fit well to a bi-exponential fit as would be expected from their bulk-like shape, but for none of them are bulk-like dynamics observed, and the longer time scale is not reliable.

# Chapter 5: Conclusions

The research presented in this thesis provides new insight into the effect of confinement on both the diffusion coefficient and reorientation times. Liquid acetonitrile confined in silica pores was studied in detail and the common models for confined dynamics examined. The results show the inaccuracy of the most ubiquitous model. In particular, the largest contributor for confined reorientational retardation is electrostatic interactions between the solvent molecules and pore wall, and molecules within the confined framework do not reach bulk-like behavior in any section of the pore or under hydrophobic conditions.

## 1. Diffusion coefficient

After careful inspection across the pores and within Pore 01, the diffusion coefficient in confined acetonitrile was found to have dramatic differences compared to bulk liquid. Diffusion is slowed because the pore wall is hydrophilic and therefore has strong interactions with polar acetonitrile. Simulations were confirmed to be reliable relative to other simulation and experimental results, where available, velocity autocorrelation functions were used to confirm the validity of the mean squared displacement method.

When considering the pores, the direction of the diffusion matters. Because the pores are aligned along the *z*-axis with periodic boundary conditions in that direction, the faster diffusion would be expected in that direction, and that is in fact the case. Most of the pore molecules are next to the wall, so they are hindered in the *x*- and *y*-directions

on one side while they are freer to move in the *z*-direction. Some exceptions do exist because the pore surface is rough therefore it has some outcroppings that potentially hinder *z*-direction movement as well.

Comparing the results from the ten different pores finds little variation, and the relative standard deviation of the diffusion constant across the pores is less than 10%. Because of this, Pore 01 was used for further analyses to represent the confined solvent. Though the choice of Pore 01 was arbitrary initially, after data inspection it appears to be a good representation in that its dynamics information is close to the average of the pores.

After the difference between confined $CH_3CN$ and bulk $CH_3CN$ was established, a more detailed explanation for the extent of the differences based on molecule placement within the pore was sought. Dividing the acetonitrile molecules into layers based on radial distance from the center is computationally simple, but was found to be significantly less meaningful than separating the layers relative to the pore wall. When considering the layers relative to the pore wall, more than 50% are within the first two layers (or 3 Å) of an oxygen atom. Another large portion is present between 3-5 Å (26.8%) where a shoulder exists (refer to **Figure 3.12**).

The diffusion coefficient of the molecules changes according to where they are located within the pore, and it also changes based on the direction of diffusion. As the molecules are located further from the pore wall, this difference is more noticeable with a percent increase in diffusion coefficient for *z*-diffusion compared to diffusion in three dimensions ranging from 19.5% when next to the pore wall up to 23.7% for inner layers.

Next, pore charge effects were studied by setting the charges on the pore atoms to zero. The diffusion coefficient increased in this neutral pore to $1.62(3) \times 10^{-9}\, m^2/s$ from $1.36(4) \times 10^{-9}\, m^2/s$, a 19% increase. The other major effect seen from turning pore charges off was how the pore molecules were distributed within the pore. By making the pore wall hydrophobic, the number of molecules in the first layer (within 2 Å of the nearest pore oxygen) decreased by nearly one-half. However, the next layer contains more molecules than it did in the charged pore, so the total number of molecules in the two layers closest to the pore wall still accounts for 50% of the total. The populations of the other layers in the uncharged pore are slightly more linearly related to the pore radius in which they are located leading to the belief that the uncharged pore's solvent molecules are somewhat less ordered than its charged counterpart. That is, the density is constant in the inner layers for the uncharged pore while some layering is still present in the charged pore.

As would be expected, temperature plays a role in the magnitude of the diffusion coefficient. As temperature increases, the molecules diffuse more quickly in the pore and have a higher diffusion coefficient. However, the distribution of the molecules at different temperatures is not necessarily intuitive. As the molecules cool they slow their diffusion and have a slightly larger propensity to populate the first layer next to the pore surface than their warmer counterparts.

## 2. Reorientational Correlation

Reorientational correlation time was the other dynamical constant of interest in the simulations. As was done for diffusion, a comparison to previously completed studies of the reorientational correlation for bulk acetonitrile was executed and found to

have similar results to those studies in bulk liquid acetonitrile.[10] The reorientational correlation function has a much slower reorientation time in the confined acetonitrile a compared to the bulk, and at least one additional time scale is present in the confined solvent. In bulk liquid $CH_3CN$, reorientational times can be broken into two time scales, an inertial component and reorientational component. For confined liquid acetonitrile, a third time scale is needed to calculate the reorientational correlation times. This added time scale is long; even after up to a nanosecond, molecules within 3-5 Å are correlated to their original positions when in a confined environment.

Separating the time scales is still a challenge, but analyzing the results for layers relative to the pore wall provides a step in that direction. The inner layers did not contain a third time scale to a significant degree while as the layers moved closer to the pore wall, the long time scale increased its contribution. Molecules do not have a definite line at which they begin to have another time scale due to the pore wall effects. This is at odds with the commonly used two-state model. The cause of the long time scale was investigated by analyzing the reorientational autocorrelation function of acetonitrile in the uncharged pore.

A large difference is seen in the reorientational autocorrelation curve of the solvent molecules after the pore charges are removed. Rather than keeping some correlation to their initial orientations for a full nanosecond, the solvent molecules are not correlated to their original values within 200 ps of the beginning of the correlation. This conclusion is true independent of the layer to which the molecules belong. Obviously, electrostatic interactions account largely for the reorientation times for acetonitrile in this environment.

## 3. Future Work

The potential for this work is far from exhausted. The best way to visualize the density within the pores is intricate due to the complexity of finding a definite pore wall edge. Some analyses have been attempted, but none have resulted in conclusive results. Because atoms are not hard spheres and instead have Lennard-Jones potentials, they are soft, so solvents, especially those like acetonitrile that are attracted to the wall, can overcome repulsion barriers.

The pores themselves may also be modified. Other pore models have already been developed using tert-butyl-terminated groups rather than hydroxyl-terminated silica. The size of the pores can vary as well, and three different pore sizes are available and ready for simulations at present.

Another area of possible future work is in elucidating the behavior of different solute molecules inside the pore with acetonitrile as the solvent. This is relatively simple, and in fact the analysis for some common small molecules has begun as of the writing of this document. However, more information is needed regarding distribution, bonding interactions and intra-/intermolecular forces before conclusions are reached.

Finally, other solvent molecules of interest may be tested to discover which trends are exclusively due to acetonitrile and which are due to confinement or properties such as having a dipole moment or the ability to accept hydrogen bonds.

# Bibliography


1. Zhang, Z.; Jonas, J. NMR Study of the Geometric Confinement Effects on the Anisotropic Rotational Diffusion of Acetonitrile-$d_3$, *J. Phys. Chem.* **1993,** *97,* 8812-8815. (Jonas)

2. Zhong, Q.; Fourkas, J. T. Optical Kerr Effect Spectroscopy of Simple Liquids. *J. Phys. Chem. B.* **2008,** *112,* 15529-15539.

3. Farrer, R. A.; Fourkas, J. T. Orientation Dynamics of Liquids Confined in Nanoporous Sol-Gel Glasses Studied by Optical Kerr Effect Spectroscopy. *Acc. Chem. Res.* **2003,** *36,* 605-612.

4. Kittaka, S.; Iwashita, T.; Serizawa, A.; Kranishi, M.; Takahara, S.; Kuroda, Y.; Mori, T.; Yamaguchi, T. Low Temperature Properties of Acetonitrile Confined MCM-41. *J. Phys. Chem. B.* **2005,** *109,* 23162-23169.

5. Takahara, S.; Nakano, M.; Kittaka, S.; Kuroda, Y.; Mori, T.; Hamano, H.; Yamaguchi, T. Neutron Scattering Study on Dynamics of Water Molecules in MCM-41. *J. Phys. Chem. B.* **1999,** *103,* 5814-5819.

6. Borguet, H. W.; Yan, E. C. Y.; Zhang, D.; Gutow, J.; Eisenthal, K. B. Molecules at Liquid and Solid Surfaces. *Langmuir*. **1998,** *14,* 1472-1477.

7. Nikiel, L.; Hopkins, B.; Zerda, T. W. Rotational and Vibrational Relaxation of Small Molecules in Porous Silica Gels. *J. Phys. Chem.* **1990,** *94,* 7458-7464.

8. Koone, N.; Shao, Y.; Zerda, T. W. Diffusion of Simple Liquids in Porous Sol-Gel Glass. *J. Phys. Chem.* **1995,** *99,* 16976-16981.

9. Allen, M. P.; Tildesley, D. J. *Computer Simulation of Liquids*; Oxford University Press, Inc.: New York, 1987.

10. Farrer, R. A.; Loughnane, B. J.; Fourkas, J. T. Dynamics of Confined Carbon Disulfide from 165 to 310 K. *J. Phys. Chem.* **1997,** *101,* 4005-4010.

11. Sivia, D. S.; Carlile, C. J.; Howells, W. S.; König, S. *Physica B* **1992,** *182,* 341-348.

12. Levchenko, A. A.; Jain, P.; Trofymluk, O.; Yu, P.; Navrotsky, A.; Sen, S. Nature of Molecular Rotation in Supercooled Glycerol under Nanoconfinement. *J. Phys. Chem. B*. **2010,** *114,* 3070-3074.

13. Piletic, I. R.; Moilanen, D. E.; Spry, D. B.; Levinger, N. E.; Fayer, M. D. Testing the Core/Shell Model of Nanoconfined Water in Reverse Micelles Using Linear and Nonlinear IR Spectroscopy, *J. Phys. Chem. A* **2006,** *110,* 4985-4999.

14. The DL_POLY Molecular Simulation Package. http://www.ccp5.ac.uk/DL_POLY.

15. Gee, P. J.; van Gunsteren, W. F. Acetonitrile Revisited: a Molecular Dynamics Study of the Liquid Phase. *Mol. Phys*. **2005,** *104*, 477-483.

16. Gulmen, T.S.; Thompson, W.H. Testing a Two-State Model of Nanoconfined Liquids: Conformational Equilibrium of Ethylene Glycol in Amorphous Silica Pores, *Langmuir.* **2006,** *22,* 10919-10923.

17. Gulmen, T. S.; Thompson, W. H. Grand Canonical Monte Carlo Simulations of Acetonitrile Filling of Silica Pores at Varying Hydrophilicity/Hydrophobicity. *Langmuir*. **2009,** *25*, 1103-1111.

18. Shoemaker, D.P. *Experiments in Physical Chemistry;* Garland, C. W.; Nibler, J. W., 3rd ed.; McGraw-Hill Companies, 1995.

19. Edwards, D. M. F.; Madden, P. A.; McDonald, I. R. A Computer Simulation Study of the Dielectric Properties of a Model of Methyl Cyanide. *Mol. Phys.,* **1984,** *51,* 1141.

20. Jorgensen, W. L.; Briggs, J. M. Monte Carlo Simulations of Liquid Acetonitrile with a Three-site Model. *Mol. Phys.,* **1988,** *63,* 547.

21. Guàrdia, E.; Pinzón, R.; Casulleras, J.; Orozco, M.; Luque, F. J. Comparison of Different Three-site Interaction Potentials for Liquid Acetonitrile. *Mol. Simulation,* **2001,** *26,* 287-306.

22. Yuan, P.; Schwartz, M. Molecular reorientation in Acetonitrile. A comparison of diffusion coefficients from Raman bandshapes an dnuclear magnetic resonance relaxation times, *J. Chem. Soc.-Faraday Trans.,* **1990,** *86,* 593.

23. Sugitani, A.; Ikawa, S.; Konaka, S. Effect of temperature on the infrared band shapes and reorientational and vibrational relaxation of liquid acetonitrile, *Chem. Phys.,* **1990,** *142,* 423.

24. Kovacs, H.; Kowalewski, J.; Maliniak, A.; Stilbs, P. Multinuclear relaxation and NMR self-diffusion study of the molecular dynamics in acetonitrile-chloroform liquid mixtures, *J. Phys. Chem.,* **1989,** *93,* 962.

25. Loughnane, B. J.; Scodinu, A.; Farrer, R. A.; Fourkas, J. T.; Mohanty, U. Exponential intermolecular dynamics in optical Kerr effect spectroscopy of small-molecule liquids, *J. Chem. Phys.,* **1999,** *111,* 2686-2694.